## 1. Introduction

Several organic proxies, based on different lipids, have been developed for estimating sea surface temperatures (SST) (Brassell et al., 1986; Schouten et al., 2002; Rampen et al., 2012). One of the first organic temperature proxies developed was the $U^{K'}_{37}$ index (Prahl and Wakeham, 1987), which is based on the relative abundances of $C_{37}$ di- and tri-unsaturated long-chain ketones. Culture and core top studies demonstrated that haptophyte algae adjust the degree of alkenone unsaturation in response to their growth temperature, and the $U^{K'}_{37}$ index is strongly related with average annual mean SST (Prahl and Wakeham, 1987; Müller et al., 1998). However, the $U^{K'}_{37}$ index may be affected by variations in nutrient concentrations, light limitation, and diagenesis (e.g. Hoefs et al., 1998; Gong and Hollander, 1999; Prahl et al., 2003; Rontani et al., 2013).

Another organic temperature proxy commonly used in the last decade is the $TEX_{86}$ (Schouten et al., 2002, 2013) based on a ratio of glycerol dialkyl glycerol tetraethers (GDGTs) with a varying number of cyclopentane moieties in the membrane lipids of marine Thaumarchaeota (Sinninghe Damsté et al., 2002). The $TEX_{86}$ is strongly correlated with satellite-derived annual mean SST in global core-top datasets (Kim et al., 2008, 2010; Ho et al., 2014). However, marine Thaumarchaeota occur throughout the whole water column (e.g., Karner et al., 2001), and thus the $TEX_{86}$ is often reflecting the water temperature of subsurface water masses (e.g., Huguet et al., 2007). The $TEX_{86}$-SST calibrations by Kim et al. (2010) distinguish between low temperature (<15ºC, $TEX^{L}_{86}$) and high temperature (>15ºC, $TEX^{H}_{86}$) regions, which takes into account an increased relative abundance of the crenarchaeol regioisomer in tropical regions. Furthermore, a subsequent re-calibration of $TEX^{L}_{86}$ with depth-integrated annual mean temperatures from 0 to 200 m water depth was established following evidence of abundant subsurface Thaumarchaeota in Antarctic regions (Kim et al., 2012b). The $TEX_{86}$ seems to be less

affected by diagenesis than the $U^{K'}_{37}$ index (Schouten et al., 2004; Kim et al., 2009b), but it can be biased by contributions of soil-derived isoprenoid GDGTs in coastal marine sediments, which can be assessed by the BIT (Branched and Isoprenoids Tetraether) index (Hopmans et al., 2004). A terrestrial effect on $TEX_{86}$ may be substantial when BIT values are >0.3 (Weijers et al., 2006, 2009), although it has been noted that this threshold depends on the location (cf. Schouten et al., 2013). More clues may be obtained by correlating the BIT index with $TEX_{86}$ values, where a significant correlation could indicate an impact of terrestrial input.

Recently, Rampen et al. (2012) proposed the long chain diol index (LDI), based on the fractional abundances of $C_{30}$ 1,15-alkyl diol relative to those of $C_{28}$ 1,13-, $C_{30}$ 1,13- and $C_{30}$ 1,15-alkyl diols (hereafter referred as diols), showing a strong correlation with annual mean SST in globally distributed surface sediments. The LDI proxy seems to be independent of salinity but the effect of degradation or nutrient limitation is not yet known. $C_{28}$ and $C_{30}$ 1,13-diols and $C_{30}$ and $C_{32}$ 1,15-diols have been reported in eustigmatophyte algae (Volkman et al., 1992, 1999; Gelin et al., 1997; Méjanelle et al., 2003) but since these algae are not widely reported from open ocean settings and the diol distributions in cultured eustigmatophytes differ from those found in the natural environment, there are still uncertainties about the biological source of long chain 1,13- and 1,15-diols in marine sediments (Versteegh et al., 1997, 2000; Rampen et al., 2012). Besides 1,13- and 1,15-diols, 1,14-diols have also been identified in marine sediments. Those lipids have been reported in *Proboscia* diatoms, which are thought to be their source (Sinninghe Damsté et al., 2003; Rampen et al., 2007), although they have also been identified in the marine alga *Apedinella radians* (Rampen et al., 2011).

SST reconstructions derived from the various organic molecular proxies can differ as proxies may reflect temperatures of different seasons or different habitat depths, and

proxies may also be affected by environmental factors other than temperature. Importantly, the use of organic proxies at high latitude regions is often problematic. Previous studies have raised doubts about the applicability of alkenone paleothermometry at high latitudes, due to the nonlinearity of the relationship of $U^{K'}_{37}$ index with SST at low temperatures (<6°C) and the high, erratic abundance of the $C_{37:4}$ alkenone (e.g., Sikes and Volkman, 1993; Rosell-Melé et al., 1994; Rosell-Melé, 1998; Rosell-Melé and Comes, 1999; Conte et al., 2006). Concerning the $TEX_{86}$, studies in subpolar regions have observed significant deviations in reconstructed SST, even with the $TEX^{L}_{86}$ calibration, (Ho et al., 2014 and references therein) as well as a substantial scatter in the correlation (Kim et al., 2010). The LDI has been applied thus far in the mid-latitudes of the Northern (Rampen et al., 2012; Lopes dos Santos et al., 2013; Rodrigo-Gámiz et al., 2014) and Southern Hemispheres (Smith et al., 2013) but not in high latitude regions, although surface sediments from high latitudes were included in the surface sediment calibration (cf. Rampen et al., 2012).

To test and constrain the application of the different organic temperature proxies at high latitudes, we have collected suspended particulate matter, sedimenting particles, and marine surface sediments from several stations distributed around Iceland. This region is of particular interest for climate studies because it is in the transition zone between polar and temperate climate regimes, thereby subjected to large variations in hydrographic conditions (Ólafsson, 1999). Thus, this high latitude region presents an ideal setting for testing and applying organic temperature proxies, including the novel LDI, in cold regions.

## 2. Material and methods

### *2.1. Oceanographic setting*

The oceanographic configuration around Iceland is predominantly characterized by the interplay of two water masses, i.e., warm and saltier Atlantic water versus cold Arctic

or subpolar waters. From the South flows the Irminger Current (IC)—a branch of the warm and salty Atlantic Current, which moves northwards along the West Iceland coast and continues along the North Iceland coast, extending down to several hundred meters (Hopkins, 1991) (Fig. 1). Flowing southward from North to West Iceland, the East Greenland Current (EGC) transports cold and low-salinity polar waters. A branch of the EGC, the East Iceland Current (EIC), turns eastward and flows southward along the East coast of Iceland (Hopkins, 1991). The EGC carries icebergs and sea ice formed in the Arctic Ocean and in East Greenland fjords (Sigtryggsson, 1972). The wide transitional zone between the polar waters and the Atlantic waters in the Denmark Strait is defined as the Polar Front. The position of this front is known to vary on annual, interannual and longer time scales (Malmberg and Jónsson 1997; Sigtryggsson, 1972). During episodes of extensive sea ice, the contribution of polar waters from the EGC to EIC is relatively large and responsible for carrying sea ice, icebergs and cold, low-salinity waters to the northwest coast of Iceland (Sigtryggsson, 1972).

The Polar Front is also expressed in the phytoplankton blooms around Iceland. In the Arctic or subpolar waters, the early onset of stratification in spring gives rise to a rapid shallowing of the mixed layer and triggers the early spring bloom (in early April) north of Iceland. In the south of Iceland, longer daylight and the warming of surface layers lead to stratification of the water column in the Atlantic water and an associated deep mixed layer, delaying the spring bloom (e.g. Zhai et al., 2012 and references therein). The spring bloom initiation varies up to a month between different regions around Iceland. Within the southern Iceland shelf region, the spring bloom generally starts in near-shore waters (mid-May) and is delayed with increasing distance from the coast, where it is affected by the interaction between runoff and wind regime (Thordardottir, 1986).

101 *2.2. Sample collection*

102 Sample material was collected around Iceland during Long Chain Diol Cruises
103 (Cruise Report 64PE341; de Haas, 2011, and Cruise Report 64PE357; Baas and Koning,
104 2012) in summer of 2011 and 2012 on board of the R/V Pelagia (Fig. 1, Table 1). During
105 July 2011, suspended particulate matter (SPM) from ca. 5 m water depth and surface
106 sediments were collected at different stations (St) around Iceland (Table 1), and a sediment
107 trap was deployed at 1850 m water depth at St 1, located in the northern part of the Iceland
108 Basin, to recover sinking particulate matter (Fig. 1). During July 2012, SPM was collected
109 at 20 and 50 m water depth at a transect from the site of the sediment trap deployment to
110 Reykjavik (Fig. 1, Table 1) after the sediment trap was recovered.

111 SPM was obtained by filtering over 142 mm diameter glass-fiber filters (GFFs)
112 with a pore diameter of 0.7 µm using a McLane Research Laboratories WTS 6-1-142LV in
113 situ pump installed on a CTD rosette frame. The CTD measured the vertical distribution of
114 temperature, salinity, turbidity, oxygen and fluorescence. SPM filters were frozen directly
115 after filtration and stored at -20ºC until analysis.

116 A McLane Parflux 78H-21 sediment trap was set to collect sinking material each
117 17.5 days in a 21-cup automated sampling carousel covering one complete annual cycle
118 (Table 2). Prior to mooring the sediment trap, the sample cups were filled with a mercuric
119 chloride-poisoned and borax-buffered solution of seawater collected from the deployment
120 depth (1 g $l^{-1}$ of $HgCl_2$; pH~8.5). After recovery of the sediment trap, collecting cups were
121 stored in the dark at 4°C.

122 Surface sediment samples were taken using a multicorer, sliced in 1 cm intervals
123 and frozen onboard.

124

125 *2.3. Extraction and lipid fractionation*

In the laboratory, any larger ‘‘swimmers’’ were removed from the sediment trap collecting cups prior to subdividing into two volumetrically split aliquots using a Folsom wet-splitter (Sell and Evans, 1982) with a precision of >95%. One half was stored in the dark at 4°C, and the second half was used for lipid analysis. The trap material was centrifuged at 3000 rpm for 15 min, followed by pipetting the water layer and washing with bidistilled $H_2O$ (3x) to remove $HgCl_2$ and borax solution. The sediment trap samples (n = 21) and surface sediment samples (n = 10) were freeze-dried, homogenized in agate mortar and extracted after addition of extracted diatomaceous earth in an Accelerated Solvent Extractor 350 (ASE 350, DIONEX) using a solvent mixture of 9:1 (v:v) dichloromethane (DCM) to methanol (MeOH) at 100ºC and 7.6 x $10^6$ Pa. The solvent from all the extracts was reduced by TurboVap LV Caliper, dried over $Na_2SO_4$ and concentrated under a stream of $N_2$ yielding a total lipid extract (TLE). To the sediment trap samples, three internal standards were added to the TLE, i.e. 10-nonadecanone ($C_{19}$ ketone) for alkenones, $C_{22}$ 7,16-diol for long chain diols and the $C_{46}$ glycerol trialkyl glycerol tetraether (GTGT) for GDGTs (Huguet et al., 2006b). Activated copper and DCM were added to the TLEs of the sediment trap samples that were found to contain elemental sulphur. After stirring overnight with a small stirring bar, the TLEs were filtered over a pipette column containing $Na_2SO_4$ and dried under a stream of $N_2$.

SPM filters (n = 14) were freeze-dried and half of each filter was saponified according to de Leeuw et al. (1983), by refluxing for 1 h with 1 M KOH in MeOH (96%). After cooling, the solvent was acidified with 2 N HCl in MeOH (1:1, v:v) to pH 2, and transferred to a separatory funnel containing bidistilled $H_2O$. The residual filters were further extracted using $H_2O$:MeOH (1:1, v:v, x1), MeOH (x1) and DCM (x3), and all solvents were combined in the separatory funnel. The DCM layer in the separatory funnel was separated from the $H_2O$:MeOH layer and the remaining $H_2O$:MeOH layer was

151 extracted three times with DCM. DCM layers were combined and rotary evaporated to
152 near dryness. Thereafter, the obtained extracts were acid hydrolyzed (3 h reflux with 2 N
153 HCl:MeOH, 1:1, v:v) and neutralized with 1 M KOH in MeOH (96%). 3 ml bidistilled
154 $H_2O$ was added to the acid hydrolyzed extracts and the lipids were extracted using DCM
155 (4×). The filter material remaining after base hydrolysis was also acid hydrolyzed as
156 described for the extracts. Subsequently, the acid-hydrolyzed residual filters were extracted
157 using $H_2O$:MeOH (1:1, v:v, x1), MeOH (x1) and DCM (x3), and the extracts were
158 combined in the separatory funnel containing bidistilled $H_2O$. The DCM layer was
159 collected and the remaining $H_2O$:MeOH layer was extracted three times with DCM. All
160 extracts, obtained by saponification and acid hydrolysis, were combined, dried under $N_2$,
161 eluted in DCM over a pipette column containing $Na_2SO_4$ and dried under a stream of $N_2$.
162 Extracts of SPM, descending particles and surface sediments were separated into
163 apolar, ketone (containing alkenones) and polar fractions (containing GDGTs and long
164 chain diols) by column chromatography using a Pasteur pipette filled with $Al_2O_3$ (activated
165 for 2 h at 150ºC) using 9:1 (v:v) hexane:DCM, 1:1 (v:v) hexane:DCM, and 1:1 (v:v)
166 DCM:MeOH as the eluents, respectively.
167
168 *2.3.1. Alkenone analysis*
169 The ketone fractions were dried under $N_2$ and re-dissolved in an appropriate volume
170 (20-100 µl) of hexane. Analysis of the di- ($C_{37:2}$) and tri-unsaturated ($C_{37:3}$) alkenones was
171 performed on an Hewlett Packard 6890 gas chromatograph (GC) using a 50-m CP Sil-5
172 column (0.32-mm diameter, film thickness of 0.12 µm), equipped with flame ionization
173 detector and helium as the carrier gas. The temperature of the oven was initially 70°C and
174 increased with a rate of 20°C per min to 200°C and subsequently with a rate of 3°C per

175 min to 320°C, at which it was held for 25 min. Alkenone relative abundances were
176 determined by integration of relevant peak areas.
177 The $U^{K'}_{37}$ index (Eq. 1) was used to estimate SSTs according to the equation by
178 Prahl and Wakeham (1987):
179
180 $U^{K'}_{37} = [C_{37:2}]/([C_{37:2}] + [C_{37:3}])$ (1)
181
182 $U^{K'}_{37}$ values were converted to SSTs using the global core top calibration of Müller
183 et al. (1998):
184
185 $U^{K'}_{37} = 0.033 \times SST + 0.044$ (2)
186
187 Five samples were run in duplicate resulting in a standard deviation (SD) of 0.02 or
188 better, equivalent to 0.8°C.
189
190 *2.3.2. GDGT analysis*
191 Polar fractions of the extracts, containing the GDGTs, were dried under a stream of
192 $N_2$, redissolved by sonication (5 min) in 200 µl hexane/propanol (99:1, v:v), and filtered
193 through 0.45 µm polytetrafluoroethylene (PTFE) filters. GDGTs were analyzed by high-
194 performance liquid chromatography–mass spectrometry (HPLC/MS) following the method
195 described by Schouten et al. (2007). Samples were analyzed on an Agilent 1100 series
196 LC/MSD SL. A Prevail Cyano column (150 mm × 2.1 mm, 3 mm) was used with
197 hexane:isopropanol (99:1, v:v) as an eluent. After the first 5 min, the eluent increased by a
198 linear gradient up to 1.8% isopropanol (vol) over the next 45 min at a flow rate of 0.2 ml
199 $min^{-1}$. Scanning was performed in single ion monitoring (SIM) mode. Identification and

quantification of the GDGT isomers and $C_{46}$ GTGT standard was achieved by integrating the peak areas of relevant peaks in m/z 1302, 1300, 1298, 1296, 1292, 1050, 1036, 1022 and 744 mass chromatograms.

The $TEX_{86}$ and $TEX^{L}_{86}$ index were calculated following Kim et al. (2010):

$$TEX_{86} = ([GDGT\ 2] + [GDGT\ 3] + [cren'] / ([GDGT\ 1] + [GDGT\ 2] + [GDGT\ 3] + [cren']) \quad (3)$$

$$TEX^{L}_{86} = ([GDGT\ 2] / ([GDGT\ 1] + [GDGT\ 2] + [GDGT\ 3]) \quad (4)$$

where numbers correspond to isoprenoid GDGTs from marine Thaumarchaeota with 1, 2 or 3 cyclopentane moieties, and cren' corresponds to crenarchaeol regioisomer, which has the antiparallel configuration of crenarchaeol (Sinninghe Damsté et al., 2002).

$TEX_{86}$ and $TEX^{L}_{86}$ values were converted to SSTs using calibrations (Eq. 5, 6) proposed by Kim et al. (2010):

$$SST = 81.5 \times TEX_{86} - 26.6 \quad (5)$$

$$SST = 67.5 \times \log(TEX^{L}_{86}) + 46.9 \quad (6)$$

Calibration errors are 5.2° and 4°C, respectively, due to the large scatter in the polar regions (Kim et al., 2010).

Furthermore, the Kim et al. (2012b) $TEX^{L}_{86}$ temperature calibration with 0-200 m water depth was also used:

$$T\ (0\text{-}200\ m) = 50.8 \times \log(TEX^{L}_{86}) + 36.1 \quad (7)$$

The Branched and Isoprenoid Tetraether (BIT) index, a measure for soil versus marine organic matter input in marine sediments, was calculated according to Hopmans et al. (2004):

$$BIT = ([GDGT\text{-}I] + [GDGT\text{-}II] + [GDGT\text{-}III]) / ([crenarchaeol] + [GDGT\text{-}I] + [GDGT\text{-}II] + [GDGT\text{-}III]) \quad (8)$$

where roman numerals correspond to the major branched GDGTs (see Hopmans et al., 2004).

A total of 17 samples were run in duplicate for $TEX_{86}$ and the BIT, showing an SD 0.09, equivalent to 1.0°C or better for $TEX^{L}_{86}$, and an SD of 0.002 or better for the BIT index.

*2.3.3. Long chain diol analysis*

After GDGT analysis, polar fractions were silylated by adding 15 µl N,O-bis(trimethylsilyl)trifluoroacetamide (BSTFA) and pyridine and heating in an oven at 60°C for 20 min. Long chain diol distributions were analyzed using a Thermo Trace Gas Chromatograph (GC) Ultra coupled to Thermo DSQ mass spectrometer (MS). A 25-m CP Sil-5 fused silica capillary column was used (25 m x 0.32 mm; film thickness = 0.12 µm)

with helium as the carrier gas. The column was directly inserted into the electron impact ion source of the DSQ quadrupole MS with an ionization energy of 70 eV. Samples were dissolved in 50-100 µl ethyl acetate and injected at 70°C. The oven was programmed to increase first at a rate of 20°C per min to 130°C, and then at a rate of 4°C per min to the final temperature of 320°C (held 25 min). Various long chain diols and the $C_{22}$ 7,16-diol standard were quantified using SIM of m/z 299, 313, 327, 341, and 187, respectively (cf. Rampen et al., 2012). The selected ions contributed on average 6.5% to the total ion counts for unsaturated long chain diols, 9.7% to the total ion counts for the saturated long chain diols, and 19% to the total ion counts for the $C_{22}$ 7,16-diol standard.

The Long chain Diol Index (LDI) was calculated and converted to SST following Rampen et al. (2012):

$$LDI = [C_{30}\ 1,15\text{-diol}] / ([C_{28}\ 1,13\text{-diol}] + [C_{30}\ 1,13\text{-diol}] + [C_{30}\ 1,15\text{-diol}]) \quad (9)$$

$$LDI = 0.033 \times SST + 0.095 \quad (10)$$

Replicate analysis of 3 samples showed a mean SD of 0.023, equivalent to 0.7°C.

## 3. Results

### *3.1. Suspended particulate matter (SPM)*

SPM was collected during two cruises, in July 2011 at six stations around Iceland at ca. 5 m water depth, and in July 2012 in a transect (St A-G) from the northern of the Iceland Basin to Reykjavik at 50 m and, at some locations, also at 20 m water depth (Fig. 1).

Alkenones were detected in all samples except from St 13. Values for the $U^{K'}_{37}$ index varied between 0.26 and 0.53 (or 6.4° to 14.7°C when translated to temperature) in the SPM around Iceland during summer 2011 (Fig. 2a, open green diamonds) and between 0.26 and 0.45 (corresponding to 6.5° to 12.5°C) during summer 2012 (Fig. 2b, open green diamonds). GDGTs were detected in all samples and the $TEX_{86}$ values ranged between 0.49 and 0.55 (corresponding to 13.1° to 17.9°C) in SPM around Iceland (Fig. 2a, dark blue circles) and between 0.34 and 0.50 (corresponding to 1.0° to 14.4°C) along the transect of 2012 (Fig. 2b, dark blue circles). $TEX^{L}_{86}$ varied between 0.28 and 0.32 (corresponding to 9.4° to 13.7°C) around Iceland (Fig. 2a, open blue circles) and between 0.22 and 0.29 (corresponding to 2.5° to 10.6°C) along the transect (Fig. 2b, open blue circles). Long chain alkyl diols were not detected in SPM around Iceland collected during summer 2011 (Fig. 2a), while $C_{28}$ and $C_{30}$ 1,13- and 1,14-diols, and $C_{30}$ and $C_{32}$ 1,15-diols were only detected in SPM collected at St A, B, F and G during the transect in the summer of 2012. LDI values varied between 0.08 and 0.49 (Fig. 2b, open brown squares) or -0.4° to 12°C when converted into temperature.

*3.2. Descending particulate matter*

Sinking particulate matter was collected between July 15, 2011 and July 16, 2012 at St 1, using a sediment trap deployed at 1850 m water depth. Bulk sediment fluxes varied between 4 and 165 mg $m^{-2}$ $day^{-1}$ (Fig. 3b), with high fluxes collected in July, September and October 2011, and from May to July 2012. $C_{37}$ alkenone fluxes varied between 0.02 and 130 μg $m^{-2}$ $day^{-1}$, peaking during spring-summer seasons, i.e. in July 2011 and in May and June 2012 (Table 2; Fig. 3c). Fluxes of the GDGTs used for the calculation of the $TEX_{86}$ index ranged between 53 and 2300 μg $m^{-2}$ $day^{-1}$ with highest values from May to June 2012 (Table 2; Fig. 3d). GDGT-0 and crenarchaeol fluxes followed the same pattern

298 as those of the GDGTs used in the $TEX_{86}$, ranging from minimum values of ca. 170 µg $m^{-2}$
299 $day^{-1}$ to maximum of 15 and 11 mg $m^{-2}$ $day^{-1}$, respectively (Fig. 3d). BIT values were
300 always below <0.01. Fluxes of long chain 1,13- and 1,15-diols used in the LDI were low
301 compared to alkenones and GDGT fluxes and varied between 1.5 and 170 ng $m^{-2}$ $day^{-1}$,
302 with highest values during July, September and October 2011, and from May to June 2012
303 (Table 2; Fig. 3e). Generally, the flux of the $C_{30}$ 1,15-diol was always low (up to 2 ng $m^{-2}$
304 $day^{-1}$) or even below detection limit for most of the intervals. The fluxes of saturated and
305 mono-unsaturated $C_{28}$ and $C_{30}$ 1,14-diols were substantially higher than those of the 1,13-
306 and 1,15-diols (Fig. 3e). The highest summed mass flux of the $C_{28}$ and $C_{30}$ mono-
307 unsaturated 1,14-diols was in September 2011 with a flux of 3.7 µg $m^{-2}$ $day^{-1}$ (Fig. 3e). $C_{28}$
308 and $C_{30}$ saturated 1,14-diols fluxes varied between minimum values of 3.8 ng $m^{-2}$ $day^{-1}$
309 during the second half of April and maximum of 770 ng $m^{-2}$ $day^{-1}$, with high fluxes during
310 July, September and October 2011 and May and June 2012 (Table 2; Fig. 3e).
311 $U^{K'}_{37}$-based temperatures derived from settling particles ranged from 5.3° to 11.4°C
312 (Fig. 4), with maximum values at the end of summer (September 2011) and late winter
313 (end of February 2012), and minimum values in spring (from May to June 2012) (Fig. 4,
314 green line), when the highest flux is observed. Temperature estimates based on $TEX_{86}$
315 varied between 6.8° and 9.6°C (Fig. 4, dark blue line), and those based on $TEX^{L}_{86}$ varied
316 between 12.6° and 17.5°C (Fig. 4, light blue line) with the highest values from November
317 2011 to April 2012. $TEX^{L}_{86}$-temperature estimates based on the 0-200 m calibration
318 showed absolute values ranging from 10.3° to 13.9°C (Fig. 4, red line). When it was
319 possible to determine, the LDI-based temperatures varies between -2.7°and 0.2°C (Fig. 4,
320 brown line and open squares).
321
322 *3.3. Surface sediments*

Surface sediments were collected in July 2011 from 21 stations around Iceland (Fig. 1; Table 1). The $U^{K'}_{37}$ index varied between 0.26 and 0.53 in the surface sediments yielding SST estimates between 7 and 11°C for St 13 and St 7, respectively (Fig. 5, open green diamonds). $TEX_{86}$ ranged between 0.36 and 0.44 with SST estimates between 2.4 and 9.2°C (Fig. 5, dark blue circles). $TEX^{L}_{86}$ ranged between 0.19 and 0.33, resulting in $TEX^{L}_{86}$ derived-temperatures between -1.2°C at St 13 and 14°C at St 1 (Fig. 5, open light blue circles), or between -0.1 and 11.4°C using the 0-200 m calibration (Fig. 5, open red circles). LDI values varied between 0.02 and 0.27, with SST estimates between -2.1 and 5.2°C, reaching high values in the coastal stations, St 3 and St 8 (Fig. 5, open brown squares).

## 4. Discussion

### *4.1. $U^{K'}_{37}$*

Long chain alkenones are produced by several haptophyte algal species thriving in the photic zone (Volkman et al., 1980, 1995; Marlowe et al., 1984), and are, therefore, thought to reflect SST. Although previous studies of cold polar waters (<4°C) of the North Atlantic have shown relatively high abundances of $C_{37:4}$ (e.g., Sicre et al., 2002), the $C_{37}$ alkenones in SPM, descending particles and surface sediments around Iceland comprised only $C_{37:3}$ and $C_{37:2}$ and no $C_{37:4}$ was detected. Comparison of $U^{K'}_{37}$-derived temperatures with in-situ temperatures showed generally lower $U^{K'}_{37}$-derived temperatures, differing up to 3.4°C for SPM around Iceland (Fig. 2a) and up to 6.6°C for the SPM transect (Fig. 2b). Reduced temperature differences (up to 2.6°C) were observed when we compared $U^{K'}_{37}$-derived SSTs with summer temperatures at 50 m water depth (Fig. 2b, purple crosses; derived from the World Ocean Atlas (WOA) 09 database; Locarnini et al., 2010) at which most of the SPM was recovered from the transect. Possibly, the alkenones collected in the

348 SPM were not representing recently produced material but alkenones synthesized over
349 several months. Since SPM was collected in July, the warmest month of the year, the $U^{K'}_{37}$
350 would reflect lower temperatures if the signal also reflected material synthesized in the
351 preceding colder months.

352 Interestingly, $U^{K'}_{37}$-derived SSTs of sedimenting particles also show major
353 discrepancies compared to satellite SSTs, i.e. somewhat higher $U^{K'}_{37}$-derived SSTs were
354 observed from January to mid-May (differing around 2-3°C) and lower temperatures from
355 mid-May to July (differing up to 4.9°C) (Fig. 4, green line and open diamonds) at the time
356 of the highest alkenone flux (Fig. 3c). The underestimation of temperatures by $U^{K'}_{37}$ in
357 sedimenting particles in July is consistent with the discrepancy between $U^{K'}_{37}$-derived and
358 in-situ temperature observed for SPM for the same time period. Application of the $U^{K'}_{37}$
359 SPM calibration proposed by Conte et al. (2006) also results in a general overestimation
360 (up to 2.7ºC) of $U^{K'}_{37}$-derived SSTs in both the SPM and sedimenting particles (data not
361 shown), suggesting that the difference between $U^{K'}_{37}$-derived and in-situ temperature is not
362 due to calibration issues.

363 Higher $U^{K'}_{37}$-derived SST in cold periods could perhaps be attributed to the gradual
364 sinking of alkenones that were produced in preceding warmer time periods. Similar
365 discrepancies, i.e. $U^{K'}_{37}$-SSTs overestimating in-situ winter temperatures and
366 underestimating in-situ summer temperatures in the surface mixed layer, have been
367 previously described for alkenones in sediment traps from other subpolar and mid-latitude
368 regions (e.g., Sikes et al., 2005; Harada et al., 2006; Seki et al., 2007; Yamamoto et al.,
369 2007; Lee et al., 2011). In the Mediterranean, Arabian Sea and the Pacific, $U^{K'}_{37}$-SSTs
370 lower than in situ SST during high alkenone flux have been attributed to either alkenone
371 production at the thermocline depth or nutrient deficiency (e.g., Ternois et al., 1997; Prahl
372 et al., 2000; Harada et al., 2006; Popp et al., 2006).

A compilation of previous sediment trap studies in the North Atlantic has shown that the $U^{K'}_{37}$ export signal produced in surface waters is not equivalent to the vertically transported $U^{K'}_{37}$ signal collected in the underlying sediment traps or accumulating in surface sediments (Rosell-Melé and Prahl, 2013). In the current study, the $U^{K'}_{37}$-SST value obtained for the surface sediment at St 1, ca. 10.7°C (Fig. 5), corresponds well with annual mean SST from WOA09 of 9.4°C (Locarnini et al., 2010), but is higher than the $U^{K'}_{37}$-derived temperature of the flux weighted average of our sediment trap data, 7.1°C (Table 3). This difference seems mainly due to the anomalously low $U^{K'}_{37}$-derived temperatures at the time of high alkenone fluxes. These discrepancies could result from (1) a bias from advected or resuspended alkenones by oceanic currents masking the local pattern of export production from overlying surface waters (e.g. Prahl et al., 2001), as has been previously noted in the NE Atlantic (Rosell-Melé et al., 2000); (2); an unusual subsurface production of alkenones in the summer of 2011 leading to a cold bias for that year only; or (3) selective degradation of alkenones when they are sedimenting on the sea floor (e.g. Hoefs et al., 1997; Rontani et al., 2013).

Similarities between $C_{37}$ alkenone flux patterns (Fig. 3c) and net primary production (derived from Ocean Color Web; Behrenfeld and Falkowski, 1997a) over this period (Fig. 3a) suggest that the increased alkenone fluxes are not caused by advection or subsurface production but can be linked to increased primary production in the upper water layer. By comparing proxy data and satellite SST, following the method of Fischer and Karakas (2009) and Mollenhauer et al. (2015), we calculated average sinking velocities (0-1850 m) for alkenones of ca. 230 m $d^{-1}$, which compares well with sinking rates of alkenones in the filamentous upwelling region off Cape Blanc (Müller and Fischer, 2001). Also in surface waters in the Norwegian–Iceland Seas, the abundances of coccolithophore communities are usually higher during the high bloom period (summer) than during the

low bloom period (late summer–fall) (Baumann et al., 2000). Furthermore, high alkenone fluxes have also been previously observed from April to June, with a rapid decline until August, in 1989 in the NE Atlantic (Rosell-Melé et al., 2000). Consequently, the increased flux of alkenones in spring likely reflects the spring bloom. $U^{K'}_{37}$-derived SSTs at the peak flux of alkenones thus likely reflects spring-early summer temperatures, in agreement with previous studies from high latitude sites (Sikes et al., 1997; Ternois et al., 1998; Rosell-Melé et al., 2000; Sicre et al., 2005, 2006; Conte et al., 2006; Hanna et al., 2006). Degradation during transport in the water column or in the oxic sediment layer is expected to result in higher $U^{K'}_{37}$-derived SSTs, since the $C_{37:3}$ has a higher degradation rate than $C_{37:2}$ (Prahl et al., 1988, 2003; Hoefs et al., 1998; Gong and Hollander, 1999), and this is indeed what we observe in the surface sediment compared to the flux-weighted mean (Table 3). An alteration of alkenones in the sea floor may explain the mismatch between surface sediment signal and flux-weighted mean signal. Finally, it is important to keep in mind that the data obtained with the sediment trap still only provides only a snapshot in time, while the surface sediment stores information collected over decades to centuries. Thus, the offset of the weighted average $U^{K'}_{37}$-derived SSTs may be just a particular feature for the year 2011, and not representative for what happened over the last few centuries.

To test the effect of seasonality and diagenetic alkenone alteration around Iceland, we compared $U^{K'}_{37}$-SST signals from all surface sediments with annual mean and seasonal SSTs (derived from the WOA09 database; Locarnini et al., 2010) (Fig. 6a, note color code as in Fig. 1). $U^{K'}_{37}$-derived SSTs show a good linear correlation with annual mean SSTs, although absolute temperature values are higher at each station, with temperature differences ranging from 1 to 4°C (Fig. 6a), generally higher than the calibration error, i.e. 1.5°C (Müller et al., 1998), and with the highest deviations for the most northern stations.

When we compared $U^{K'}_{37}$-derived temperature values with SST from different seasons, the best fit is obtained with the summer mean SSTs (Fig. 6b). This is in agreement with peak alkenone fluxes recorded in our sediment trap during late spring-early summer. Thus, the sedimentary signal of $U^{K'}_{37}$-SST around Iceland seems in general to reflect the maximum production season of alkenones.

*4.2. $TEX_{86}$*

GDGTs in the marine environment are likely biosynthesized by Thaumarchaeota (Sinninghe Damsté et al., 2002) that are omnipresent in the global ocean, including the polar regions (e.g., Hoefs et al., 1997; DeLong et al., 1998; Schouten et al., 2000). $TEX^{L}_{86}$ was developed for polar oceans in order to improve the correlation between $TEX_{86}$ and SST (Kim et al., 2010), but a recent study has shown that $TEX_{86}$ is still suitable as well (Ho et al., 2014). The $TEX^{L}_{86}$-SST estimates in the SPM around Iceland showed a highly variable relationship with in situ temperatures, showing temperatures up to 6°C higher values around Iceland during 2011 (Fig. 2a), while for the SPM transect, the difference with summer temperatures at 50 m water depth from WOA09 was up to 7°C lower (Fig. 2b). Even higher offsets, both positive and negative, up to 11°C, were obtained with $TEX_{86}$-SST estimates (Figs. 2a,b). A reason for the poor correspondence of $TEX_{86}$-derived temperatures with in-situ and satellite temperatures could be a depth habitat effect, since Thaumarchaeota can thrive deeper in the marine water column (Karner et al., 2001; Herndl et al., 2005), although they tend to have their highest cell numbers at depths <200 m (e.g. Karner et al., 2001). We also applied a specific $TEX_{86}$ SPM calibration proposed by Schouten et al. (2013), but temperatures still did show significant offsets with in situ temperatures (data not shown).

447 Part of the mismatch may be due to the fact that Thaumarchaeota are smaller in cell
448 size than the 0.7 µm pore diameter of the SPM filters (Könneke et al., 2005) and thus may
449 not be quantitatively captured on the GFFs (Ingalls et al., 2012), possibly affecting the
450 $TEX_{86}$ values. However, other studies have shown comparable $TEX_{86}$ values obtained with
451 both 0.7 and 0.2 µm pore diameter filters (e.g., Herfort et al., 2007) or good
452 correspondence with depth (Schouten et al., 2012) or seasonal (Pitcher et al., 2011) profiles
453 of isoprenoidal GDGT concentrations from 7 µm pore diameter filters and
454 Thaumarchaeotal rRNA gene abundances from 0.2 µm pore diameter filters. Thus, the
455 filter size is unlikely to have affected $TEX_{86}$ values. Another issue may be that we
456 analyzed saponified SPM filters, combining both intact and core (non-intact) GDGT-based
457 lipids. In the natural environment, core lipid-GDGTs are derived for a substantial portion
458 from dead cells and may thus represent a fossil signal from other areas or represent an
459 integrated annual temperature signal. Lipp and Hinrichs (2009) showed notable differences
460 in derived temperatures using core- vs. intact polar lipid-GDGTs from marine sediments.
461 Usually, $TEX_{86}$-derived temperatures are higher for IPL-GDGTs than for core-GDGTs, as
462 was observed in SPM from the Arabian Sea (Schouten et al., 2012), thus, reduced $TEX_{86}$
463 derived-SSTs from the SPM transect may related to core-GDGT contributions. However,
464 this does not fully explain the dissimilarities observed in the SPM around Iceland, and thus
465 we lack a clear explanation.
466 Regarding sedimenting particles, $TEX^{L}_{86}$-derived SSTs (Fig. 4, blue line and open
467 circles) were all much higher (up to ca. 9°C) than satellite SSTs. Reduced differences (up
468 to ca. 5°C higher than satellite SSTs) were obtained when temperature values were
469 estimated using the $TEX^{L}_{86}$ 0-200 m calibration (Kim et al., 2012b) (Fig. 4, red line and
470 open circles and dashed purple line). Interestingly, differences in temperature decreased
471 significantly when $TEX_{86}$-derived temperature and satellite derived SST were compared

472 (Fig. 4; dark blue line and filled circles), particularly during times of low GDGT fluxes
473 (Fig. 3d). During times of high GDGT fluxes, $TEX_{86}$-SST were lower than satellite SST by
474 up to 4.6°C, which may suggest that the temperature signal is not derived just from surface
475 waters. This is supported by $TEX_{86}$ temperature values from SPM collected at St 1 during
476 both cruises; $TEX_{86}$ derived temperatures from the surface waters are slightly higher than
477 the satellite SSTs, and significantly higher than the $TEX_{86}$ values derived from the material
478 collected in the same months in the sediment trap at 1850 m water depth. We observed
479 notable differences in estimated temperatures when we used different calibrations,
480 obtaining better results with the $TEX_{86}$ calibration (Kim et al., 2010). Similar findings were
481 made by Ho et al. (2014) who applied $TEX^{L}_{86}$ and $TEX_{86}$ in different polar and subpolar
482 regions, as the Pacific sector of the Southern Ocean and the Subarctic Front in the North
483 Pacific. Lateral transport of GDGTs is not likely to have an effect on $TEX_{86}$ temperatures
484 since isoprenoid GDGTs are less susceptible to long distance advection than alkenones
485 (Mollenhauer et al., 2008; Shah et al., 2008; Kim et al., 2009a). Short-term degradation has
486 also shown to have no significant impact on the $TEX_{86}$ (Schouten et al., 2004; Kim et al.,
487 2009b). Terrigenous GDGTs are also unlikely to be the reason for the offset in estimated
488 temperatures around Iceland, based on the low values of the BIT index (<0.01) (Weijers et
489 al., 2006, 2009) and the low correlation ($R^2$<0.08) between the BIT index and $TEX_{86}$
490 values (c.f. Schouten et al., 2013). Comparison of the flux weighted mean $TEX_{86}$ value
491 with surface sediment at St 1 shows similar values, independent of calibration used, i.e.
492 8.5° and 9.2°C using $TEX_{86}$-SST, 14.5° and 14.0°C using $TEX^{L}_{86}$-SST, 11.7° and 11.4°C
493 for $TEX^{L}_{86}$ 0-200 m, suggesting no alteration of the GDGT signal during transport to the
494 sea floor (Table 3).

495 GDGT fluxes were high during July, September and October 2011, followed by
496 May and June 2012 (Fig. 3d), showing similar patterns as bulk sediment flux and primary

497 production (Figs. 3a,b). Following the method of Fischer and Karakas (2009) and
498 Mollenhauer et al. (2015), we estimate average sinking velocities (0-1850 m) for GDGTs
499 of ca. 230 m $d^{-1}$.

500 The GDGT flux pattern is not entirely consistent with the ecology of marine
501 Thaumarchaeota, as their abundance is often negatively correlated with that of
502 phytoplankton, since they are chemolithoautotrophs using ammonia derived from
503 breakdown of organic matter (e.g., Massana et al., 1997; Herndl et al., 2005; Könneke et
504 al., 2005; Wuchter et al., 2006). However, the same GDGT flux pattern was also observed
505 in the Arabian Sea (Wuchter et al., 2006), the Santa Barbara basin, off the coast of
506 southern California (Huguet et al., 2007), and the upwelling region off Cape Blanc in
507 Mauritania (Mollenhauer et al., 2015), i.e. high at times of high primary productivity. This
508 was explained by a more efficient transport of thaumarchaeotal cells, and thus GDGTs, to
509 deeper waters by packaging activity of zooplankton thriving after a phytoplankton bloom.
510 This could be also the case in the northern Iceland basin, where the bulk sediment flux may
511 act as an important mechanism for transporting these lipids to the seafloor. However, the
512 fact that highest fluxes are observed in late summer does not mean that the annual $TEX_{86}$
513 signal here also represents summer temperatures, as previously suggested by Ho et al.
514 (2014) for surface sediments from the Arctic, northern Pacific and southern Ocean, since
515 the flux weighted mean $TEX_{86}$ value from the sediment trap, and the $TEX_{86}$ value from the
516 underlying sediment are both similar to annual mean SST (Table 3).

517 $TEX_{86}$- and $TEX^{L}_{86}$-derived SST in the surface sediments distributed around
518 Iceland correlate with WOA09 annual mean SSTs (Figs. 6c,e), although they do show a
519 substantial offset varying from 1 to 4.7°C. A similar fit is obtained with winter mean
520 temperatures (Figs. 6d,f), whereas the correlation with summer mean temperatures is
521 substantially poorer (data not shown). This latter observation agrees with the idea that the

highest GDGT flux during summer does not automatically result in a $TEX_{86}$ signal which is recording late summer temperatures (Fig. 3d). This is in contrast with observations by Ho et al. (2014), who showed anomalously high SST estimates in surface sediments from the Arctic, northern Pacific and southern Ocean, and obtained the best correlation of $TEX_{86}$-SSTs with summer SSTs.

To test if the sedimentary $TEX_{86}$ signal around Iceland is mainly reflecting subsurface temperature waters as suggested for some other regions (e.g., Huguet et al., 2007; Lopes dos Santos et al., 2010; Kim et al., 2012a,b), we compared $TEX^{L}_{86}$ 0-200 m temperature estimates (Kim et al., 2012b) with the temperature of the upper 200 m of the water column based on WOA09. Indeed, we obtained a better correspondence with both annual and winter mean temperatures (Figs. 6g,h), with differences ranging from 0.5 to 3.5°C. This suggests that $TEX_{86}$-derived signals in the surface sediments around Iceland may reflect subsurface (i.e. 0-200 m) temperatures.

*4.3. LDI*

Long chain alkyl diols, either the 1,13- and 1,15-diols involved in the LDI or the 1,14-diols produced by *Proboscia* diatoms (Sinninghe Damsté et al., 2003) and *Apedinella radians* (Rampen et al., 2011), were below detection limit in SPM sampled around Iceland in summer 2011. In the SPM sampled during the 2012 transect, small amounts of long chain 1,15-, 1,14- and 1,13-diols were detected. This suggests that July is not the period of highest productivity for long chain diol producers around Iceland. However, long chain 1,13- and 1,15-diol mass fluxes were relatively high during July, September and October 2011, and from May to July 2012 (Fig. 3e), suggesting that diol producers were present, although not at the time, depths or exact locations as where the SPM was sampled. This suggests a patchy distribution of diol producers. Indeed, it has been observed that diatom

distribution and composition around Iceland is highly variable and strongly influenced by different environmental variables and particularly by summer sea surface temperature (Jiang et al., 2001).

Interestingly, the fluxes of 1,13- and 1,15-diols were always much lower than $C_{28}$ and $C_{30}$ saturated and mono-unsaturated 1,14-diol fluxes, as well as three orders of magnitude lower than those of alkenones and GDGTs. This indicates that 1,13- and 1,15-diols and their producers are not very abundant in this environment. The presence of $C_{28}$ and $C_{30}$ saturated and mono-unsaturated 1,14-diol fluxes suggests that *Proboscia* diatoms have bloomed in late summer-autumn and late spring-summer. This is further supported by the identification of $C_{27}$ and $C_{29}$ mid-chain hydroxyl methyl alkanoates in the sedimenting particles (data not shown), which are also biomarker lipids from *Proboscia* diatoms (Sinninghe Damsté et al., 2003). Interestingly, trace amounts of both $C_{28}$ and $C_{30}$ 1,13-diols have been identified in *Proboscia* species (Rampen et al., 2007), and the relatively high abundance of saturated and mono-saturated 1,14-diols, combined with a similar flux pattern as that of the 1,13 and 1,15-diols, suggests that *Proboscia* may also be a source for the 1,13- and 1,15-diols in this area.

Where LDI values could be calculated for the SPM, temperatures were substantially lower than satellite SSTs (Figs. 2b), exceeding the calibration error of 2°C (Rampen et al., 2012). For the sediment trap, LDI values were not always calculated due to the non-quantifiable amount of $C_{30}$ 1,15-diol. For cases where it was possible, the temperature values were, like the SPM, much lower than satellite temperatures (Fig. 4, brown line and open squares; Table 3). The eukaryotic phytoplankton generally responsible for the production of 1,13- and 1,15-diols are likely eustigmatophyte algae, autotrophs living in the upper photic zone (Volkman et al., 1992, Rampen et al., 2012), and on a global scale, the LDI correlates best with late summer-early autumn SST (cf. Rampen et al., 2012).

572 Thus, a contribution from colder deep water is unlikely to explain the low temperatures
573 observed with the LDI. A similar observation is made for the LDI-derived SSTs in the
574 surface sediments around Iceland which are always lower than annual mean SST, even
575 when compared with the coldest season, i.e. winter mean SST (Figs. 6i,j). Furthermore,
576 there is no correlation of LDI values with SST. Also in the surface sediments, relatively
577 low abundances of 1,13- and 1,15-diols compared to 1,14-diols were observed. The
578 mismatch of LDI values with temperature as well as the low abundances of long chain
579 1,13- and 1,15-alkyl diols reinforce the hypothesis that *Proboscia* diatoms seem to be at
580 least a partial source of 1,13- and 1,15-diols in the Iceland region. This suggests that the
581 LDI may not be applicable in this region. Therefore, we advise that, if 1,14-diols dominate
582 the distributions of long chain alkyl diols, the LDI should be applied with great caution.
583

584 **5. Conclusions**

585 The application of three independent organic temperature proxies at high latitudes
586 was studied in the region around Iceland. $U^{K'}_{37}$-derived SSTs in SPM and sedimenting
587 particles are generally lower than annual mean SST. In contrast, $U^{K'}_{37}$-derived SSTs in the
588 surface sediments around Iceland correlate well with summer mean SST, which seems in
589 agreement with the observation of elevated alkenone fluxes during late spring-early
590 summer. The mismatch between the flux-weighted mean $U^{K'}_{37}$-derived SST and the $U^{K'}_{37}$-
591 derived SST from the underlying surface sediment may be due to diagenetic alkenone
592 alteration during the sedimentation process or because an unusual year was sampled with
593 the sediment trap.

594 High fluxes of the isoprenoidal GDGTs used in the $TEX_{86}$ proxy were observed
595 during warmer months with high productivity and mass fluxes, which may be explained by
596 a preferential transport of GDGTs to deeper waters by packaging activity of zooplankton

thriving after a phytoplankton bloom. However, the flux-weighted mean $TEX_{86}$ value correspond well with annual mean SST in surface sediments, $TEX_{86}$-derived temperatures showed a good correlation with both annual and winter mean 0-200 m temperatures, suggesting that the $TEX_{86}$ signal is primarily derived from these subsurface waters

The LDI around Iceland did not show any relationship with SST. The similarity in trends between all long chain alkyl diols and the dominant abundances of 1,14-diols over 1,13- and 1,15-diols may suggest that *Proboscia* diatom is an important source of 1,13- and 1,15-diols in the Iceland region, limiting the LDI application in this area. Therefore we advise caution in interpreting LDI values in areas where 1,14-diols are strongly dominating the long chain alkyl diol distributions.

*Data from this publication are archived in the data centre "Pangaea" (www.Pangaea.de).*

## Author contribution

J. S. S. D. and S. W. R. designed the research cruises. S. W. R., M. B. and H. D. H. were on board of the research cruises. M. R. G. performed the experimental laboratory work. M. R. G. prepared the manuscript with contributions from all co-authors.

## Acknowledgements

This work was supported by the Earth and Life Sciences Division of the Netherlands Organization for Scientific Research (NWO-ALW) by a grant (ALW 820.01.013) to J.S.S.D. We would like to thank onboard assistance by the crew and scientific team during cruise Long Chain Diols with R.V. Pelagia (2011, 2012). We thank Anchelique Mets and Jort Ossebaar for laboratory assistance.

621 **References**


622 Baas, M. and Koning, E., Cruise report R.V. Pelagia 64PE357, Diols-Trap Recovery, Reykjavik -
623 Reykjavik, 23-29 July 2012. http://melia.nioz.nl/public/dmg/rpt/crs/64pe357.pdf
624 Baumann, K.-H., Andruleit, H. A., and Samtleben, C.: Coccolithophores in the Nordic Seas:
625 comparison of living communities with surface sediment assemblages. Deep-Sea Res. Pt II, 47,
626 1743-1772, 2000.
627 Behrenfeld, M. J., and Falkowski, P. G.: Photosynthetic rates derived from satellite-based
628 chlorophyll concentration, Limnol. Oceanogr., 42, 1-20, 1997a.
629 Brassell, S. C., Eglinton, G., Marlowe, I. T., Pflaumann, U., and Sarnthein, M.: Molecular
630 stratigraphy: A new tool for climatic assessment, Nature, 320, 129-133, 1986.
631 Conte, M. H., Weber, J. C., King, L. L., and Wakeham, S. G.: The alkenone temperature signal in
632 western North Atlantic surface waters, Geochim. Cosmochim. Acta, 65, 4275-4287, 2001.
633 Conte, M. H., Sicre, M. -A., Rühlemann, C., Weber, J. C., Schulte, S., Schulz-Bull, D., and Blanz,
634 T.: Global temperature calibration of the alkenone unsaturation index ($U^{K'}_{37}$) in surface waters
635 and comparison with surface sediments, Geochem., Geophys., Geosyst., 7, Q02005, 2006.
636 de Haas, H., Cruise report R.V. Pelagia 64PE341, Long Chain Diols (LCD), Texel - Reykjavik, 7-
637 22 July 2011. http://melia.nioz.nl/public/dmg/rpt/crs/64pe341.pdf
638 De Leeuw, J. W., Rijpstra, W. I. C., Schenck, P. A., and Volkman, J.: Free, esterified and residual
639 sterols in Black Sea Unit I sediments, Geochim. Cosmochim. Acta, 47, 455-465, 1983.
640 DeLong, E. F., King, L. L., Massana, R., Cittone, H., Murray, A., Schleper, C., and Wakeham, S.
641 G.: Dibiphytanyl ether lipids in nonthermophilic crenarchaeotes, Appl. Environ. Microbiol., 64,
642 113-1138, 1998.
643 Fietz, S., Martínez-Garcia, A., Huguet, C., Rueda, G., and Rosell-Melé, A.: Constraints in the
644 application of the Branched and Isoprenoid Tetraether index as terrestrial input proxy, J.
645 Geophys. Res., 116, C10032, 2011.
646 Fischer, G., and Karakas, G.: Sinking rates and ballast composition of particles in the Atlantic
647 Ocean: implications for the organic carbon fluxes to the deep ocean, Biogeosciences 6, 85-102,
648 2009.
649 Gelin, F., Boogers, I., Noordeloos, A. A. M., Sinninghe Damsté, J. S., Riegman, R., and de Leeuw,
650 J. W.: Resistant biomacromolecules in marine microalgae of the classes Eustigmatophyceae
651 and Chlorophyceae: Geochemical implications, Org. Geochem., 26, 659-675, 1997.
652 Gong, C., and Hollander, D. J.: Evidence for differential degradation of alkenones under
653 contrasting bottom water oxygen conditions: Implications for paleotemperature reconstruction,
654 Geochim. Cosmochim. Acta, 63, 405-411, 1999.
655 Hanna, E., Jonsson, T., Ólafsson, J., and Vladimarsson, H.: Icelandic coastal sea surface
656 temperature records constructed: putting the pulse on air–sea climate interactions in the
657 Northern North Altantic. Part I: Comparison with HadISST1 open-ocean surface temperatures

and preliminary analysis of long-term patterns and anomalies of SSTs around Iceland. J. Clim., 19, 5652-5666, 2006.

Harada, N., Sato, M., Shiraishi, A., and Honda, M. C.: Characteristics of alkenone distributions in suspended and sinking particles in the northwestern North Pacific. Geochim. Cosmochim. Acta, 70, 2045-2062, 2006.

Herfort, L., Schouten, S., Abbas, B., Veldhuis, M. J. W., Coolen, M. J. L., Wuchter, C., Boon, J. P., Herndl, G. J., and Sinninghe Damsté, J. S.: Variations in spatial and temporal distribution of Archaea in the North Sea in relation to environmental variables, FEMS Microbiol. Ecol., 62, 242-257, 2007.

Herndl, G. J., Reinthaler, T., Teira, E., van Aken, H., Veth, C., Pernthaler, A., and Pernthaler, J.: Contribution of Archaea to total prokaryotic production in the deep Atlantic Ocean, Appl. Environ. Microbiol., 71, 2303-2309, 2005.

Ho, S. L., Mollenhauer, G., Fietz, S., Martínez-Garcia, A., Lamy, F., Rueda, G., Schipper, K., Méheust, M., Rosell-Melé, A., Stein, R., and Tiedemann, R.: Appraisal of $TEX_{86}$ and $TEX^{L}_{86}$ thermometries in subpolar and polar regions, Geochim. Cosmochim. Acta, 131, 213-226, 2014.

Hoefs, M. J. L., Schouten, S., King, L. L., Wakeham, S. G., de Leeuw, J. W., and Sinninghe Damsté, J. S.: Ether lipids of planktonic archaea in the marine water column, Appl. Environ. Microbiol., 63, 3090-3095, 1997.

Hoefs, M. J. L., Versteegh, G. J. M., Rijpstra, W. I. C., de Leeuw, J. W., and Sinninghe Damsté, J. S.: Postdepositional oxic degradation of alkenones: Implications for the measurement of palaeo sea surface temperatures, Paleoceanography, 13, 42-49, 1998.

Hopkins, T. S.: The GIN Sea—a synthesis of its physical oceanography and literature review 1972–1985, Earth Sci. Rev., 30, 175-318, 1991.

Hopmans, E. C., Weijers, J. W. H., Schefuß, E., Herfort, L., Sinninghe Damsté, J. S., and Schouten, S.: A novel proxy for terrestrial organic matter in sediments based on branched and isoprenoid tetraether lipids, Earth Planet. Sci. Lett., 224, 107-116, 2004.

Huguet, C., Hopmans, E. C., Febo-Ayala, W., Thompson, D. H., Sinninghe Damsté, J. S., and Schouten, S.: An improved method to determine the absolute abundance of glycerol dibiphytanyl glycerol tetraether lipids, Org. Geochem., 37, 1036-1041, 2006b.

Huguet, C., Schimmelmann, A., Thunell, R., Lourens, L. J., Sinninghe Damsté, J. S., and Schouten, S.: A study of the $TEX_{86}$ paleothermometer in the water column and sediments of the Santa Barbara Basin, California, Paleoceanography, 22, PA3203, 2007.

Ingalls, A. E., Huguet, C., and Truxal, L. T.: Distribution of intact and core membrane lipids of archaeal glycerol dialkyl glycerol tetraethers among size-fractionated particulate organic matter in Hood Canal, Puget Sound, Appl. Environ. Microbiol., 78, 1480-1490, 2012.

693 Jiang, H., Seidenkrantz, M. S., Knudsen, K. L., and Eiríksson, J.: Diatom surface sediment
694 assemblages around Iceland and their relationships to oceanic environmental variables, Mar.
695 Micropaleontol., 41, 73-96, 2001.
696 Karner, M. B., DeLong, E. F., and Karl, D. M.: Archaeal dominance in the mesopelagic zone of the
697 Pacific Ocean, Nature, 409, 507-510, 2001.
698 Kim, J. -H., Crosta, X., Michel, E., Schouten, S., Duprat, J., and Sinninghe Damsté, J. S.: Impact of
699 lateral transport on organic proxies in the Southern Ocean, Quat. Res., 71, 246-250, 2009a.
700 Kim, J. -H., Huguet, C., Zonneveld, K. A. F., Versteegh, G. J. M., Roeder, W., Sinninghe Damsté,
701 J. S., and Schouten, S.: An experimental field study to test the stability of lipids used for $TEX_{86}$
702 and $U^{K'}_{37}$ palaeothermometry, Geochim. Cosmochim. Acta, 73, 2888-2898, 2009b.
703 Kim, J. -H., van der Meer, J., Schouten, S., Helmke, P., Willmott, V., Sangiorgi, F., Koç, N.,
704 Hopmans, E. C., and Sinninghe Damsté, J. S.: New indices and calibrations derived from the
705 distribution of crenarchaeal isoprenoid tetraether lipids: Implications for past sea surface
706 temperature reconstructions, Geochim. Cosmochim. Acta, 74, 4639-4654, 2010.
707 Kim J. -H., Romero, O. E., Lohmann, G., Donner, B., Laepple, T., Haam, E., and Sinninghe
708 Damsté, J. S.: Pronounced subsurface cooling of North Atlantic waters off Northwest Africa
709 during Dansgaard-Oeschger interstadials, Earth Planet. Sci. Lett., 339, 95-102, 2012a.
710 Kim, J. -H., Crosta, X., Willmott, V., Renssen, H., Bonnin, J., Helmke, P., Schouten, S., and
711 Sinninghe Damsté, J. S.: Holocene subsurface temperature variability in the eastern Antarctic
712 continental margin, Geophys. Res. Lett., 39, L06705, 2012b.
713 Könneke, M., Bernhard, A. E., de la Torre, J. R., Walker, C. B., Waterbury, J. B., and Stahl, D. A.:
714 Isolation of an autotrophic ammonia-oxidizing marine archaeon, Nature, 437, 543-546, 2005.
715 Lee, K. E., Khim, B. K., Otosaka, S., and Noriki, S.: Sediment trap record of alkenones from the
716 East Sea (Japan Sea). Org. Geochem., 42, 255-261, 2011.
717 http://dx.doi.org/10.1016/j.orggeochem.2010.12.008.
718 Locarnini, R. A., Mishonov A. V., Antonov, J. I., Boyer, T. P., Garcia, H. E., Baranova, O. K.,
719 Zweng, M. M., and Johnson, D. R.: World Ocean Atlas 2009: Volume 1: Temperature, in:
720 NOAA Atlas NESDIS 68, Levitus, S. (Ed.), U.S. Government Printing Office, Washington,
721 D.C., pp. 184, 2010.
722 Lopes dos Santos, R. A., Spooner, M. I., Barrows, T. T., De Deckker, P., Sinninghe Damsté, J. S.,
723 and Schouten, S.: Comparison of organic ($U^{K'}_{37}$, $TEX^{H}_{86}$, LDI) and faunal proxies
724 (foraminiferal assemblages) for reconstruction of late Quaternary sea-surface temperature
725 variability from offshore southeastern Australia, Paleoceanography, 28, 377-387, 2013.
726 Malmberg, S. -A.: The water masses between Iceland and Greenland, J. Mar. Sci. Inst., 9, 127-140,
727 1985.
728 Malmberg, S. -A., and Jónsson, S.: Timing of deep convection in the Greenland and Iceland Seas,
729 ICES J. Mar. Sci., 54, 300-309, 1997.

730 Marlowe, I. T., Green, J. C., Neal, A. C., Brassell, S. C., Eglinton, G., and Course, P. A.: Long-
731 chain (n-$C_{37}$–$C_{39}$) alkenones in the Prymnesiophyceae. Distribution of alkenones and other
732 lipids and their taxonomic significance, Brit. Phycol. J., 19, 203-216, 1984.
733 Massana, R., Murray, A. E., Preston, C. M., and DeLong, E. F.: Vertical distribution and
734 phylogenetic characterization of marine planktonic archaea in the Santa Barbara channel, Appl.
735 Environ. Microbiol., 63, 50-56, 1997.
736 Méjanelle, L., Sanchez-Gargallo, A., Bentaleb, I., and Grimalt, J. O.: Long chain n-alkyl diols,
737 hydroxy ketones and sterols in a marine eustigmatophyte, *Nannochloropsis gaditana*, and in
738 *Brachionus plicatilis* feeding on the algae, Org. Geochem., 34, 527-538, 2003.
739 Mollenhauer, G., Eglinton, T. I., Hopmans, E. C., and Sinninghe Damsté, J. S.: A radiocarbon-
740 based assessment of the preservation characteristics of crenarchaeol and alkenones from
741 continental margin sediments, Org. Geochem., 39, 1039-1045, 2008.
742 Mollenhauer, G., Basse, A., Kim, J.-H., Sinninghe Damsté, J. S., and Fischer, G.: A four-year
743 record of $U^{K'}_{37}$- and $TEX_{86}$-derived sea surface temperature estimates from sinking particles in
744 the filamentous upwelling region off Cape Blanc, Mauritania. Deep-Sea Res. Pt I, 97, 67-79,
745 2015.
746 Müller, P. J., Kirst, G., Ruhland, G., von Storch, I., and Rossell-Melé, A.: Calibration of alkenone
747 paleotemperature index $U^{K'}_{37}$ based on core tops from the eastern South Atlantic and the global
748 ocean (60ºN–60ºS), Geochim. Cosmochim. Acta, 62, 1757-1771, 1998.
749 Müller, P. J., and Fischer, G.: A 4-year sediment trap record of alkenones from the filamentous
750 upwelling region off Cape Blanc, NW Africa and a comparison with distributions in underlying
751 sediments. Deep-Sea Res. Pt I, 48, 1877-1903, 2001.
752 Ólafsson, J.: Connections between oceanic conditions off N-Iceland, Lake Mývatn temperature,
753 regional wind direction variability and the North Atlantic Oscillation, Rit Fiskideildar, 16, 41-
754 57, 1999.
755 Pitcher, A., Wuchter, C., Siedenberg, K., Schouten, S., and Sinninghe Damsté, J. S.: Crenarchaeol
756 tracks winter blooms of ammonia-oxidizing Thaumarchaeota in the coastal North Sea, Limnol.
757 Oceanogr., 56, 2308-2318, 2011.
758 Popp, B. N., Prahl, F. G., Wallsgrove, R. J., and Tanimoto, J.: Seasonal patterns of alkenone
759 production in the subtropical oligotrophic North Pacific. Paleoceanogeaphy, 21, PA1004, 2006.
760 Prahl, F. G., and Wakeham, S.G.: Calibration of unsaturation patterns in long-chain ketone
761 compositions for paleotemperature assessment, Nature, 330, 367-369, 1987.
762 Prahl, F. G., Muehlhausen, L. A., and Zahnle, D. B.: Further evaluation of long-chain alkenones as
763 indicators of paleoceanographic conditions, Geochim. Cosmochim. Acta, 52, 2303-2310, 1988.
764 Prahl, F. G., Dymond, J., and Sparrow, M. A.: Annual biomarker record for export production in
765 the central Arabian Sea. Deep-Sea Res. Pt II, 47, 1581-1604, 2000.

766 Prahl, F. G., Pilskaln, C. H., and Sparrow, M. A.: Seasonal record for alkenones in sedimentary
767 particles from the Gulf of Maine. Deep-Sea Res. Pt I, 48, 515-528, 2001.
768 Prahl, F. G., Sparrow, M. A., and Wolfe, G. V.: Physiological impacts on alkenone
769 paleothermometry, Paleoceanography, 18, 1025, 2003.
770 Rampen, S. W., Schouten, S., Wakeham, S. G., and Sinninghe Damsté, J. S.: Seasonal and spatial
771 variation in the sources and fluxes of long chain diols and mid-chain hydroxy methyl
772 alkanoates in the Arabian Sea, Org. Geochem., 38, 165-179, 2007.
773 Rampen, S. W., Schouten, S., and Sinninghe Damsté, J. S.: Occurrence of long chain 1,14 diols in
774 *Apedinella radians*, Org. Geochem., 42, 572-574, 2011.
775 Rampen, S. W., Willmott, V., Kim, J. -H., Uliana, E., Mollenhauer, G., Schefuß, E., Sinninghe
776 Damsté, J. S., and Schouten, S.: Long chain 1,13- and 1,15-diols as a potential proxy for
777 palaeotemperature reconstruction, Geochim. Cosmochim. Acta, 84, 204-216, 2012.
778 Rodrigo-Gámiz, M., Martínez-Ruiz, F., Rampen, S. W., Schouten, S., and Sinninghe Damsté, J. S.:
779 Sea surface temperature variations in the western Mediterranean Sea over the last 20 kyr: A
780 dual-organic proxy ($U^{K'}_{37}$ and LDI) approach, Paleoceanography, 29, 87-98, 2014.
781 Rontani, J. -F., Volkman, J. K., Prahl, F. G., and Wakeham, S.G.: Biotic and abiotic degradation of
782 alkenones and implications for $U^{K'}_{37}$ paleoproxy applications: A review, Org. Geochem., 59,
783 95-113, 2013.
784 Rosell-Melé, A.: Interhemispheric appraisal of the value of alkenone indices as temperature and
785 salinity proxies in high-latitude locations, Paleoceanography, 13, 694-703, 1998.
786 Rosell-Melé, A., and Comes, P.: Evidence for a warm Last Glacial Maximum in the Nordic seas or
787 an example of shortcomings in $U^{K'}_{37}$ and $U^{K}_{37}$ to estimate low sea surface temperature?,
788 Paleoceanography, 14, 770-776, 1999.
789 Rosell-Melé, A., and Prahl, F. G.: Seasonality of $U^{K'}_{37}$ temperature estimates as inferred from
790 sediment trap data, Quat. Sci. Rev., 72, 128-136, 2013.
791 Rosell-Melé, A., Carter, J., and Eglinton, G.: Distributions of long-chain alkenones and alkyl
792 alkenoates in marine surface sediments from the North East Atlantic, Org. Geochem., 22, 501-
793 509, 1994.
794 Rosell-Melé, A., Eglinton, G., Pflaumann, U., and Sarnthein, M.: Atlantic core-top calibration of
795 the $U^{K'}_{37}$ index as a sea-surface palaeotemperature indicator, Geochim. Cosmochim. Acta, 59,
796 3099-3107, 1995.
797 Rosell-Melé, A., Comes, P., Müller, P. J., and Ziveri, P.: Alkenone fluxes and anomalous $U^{K'}_{37}$
798 values during 1989-1990 in the Northeast Atlantic (48°N 21°W), Mar. Chem., 71, 251-264,
799 2000.
800 Schouten, S., Hopmans, E. C., Pancost, R. D., and Sinninghe Damsté, J. S.: Widespread occurrence
801 of structurally diverse tetraether membrane lipids: Evidence for the ubiquitous presence of low-
802 temperature relatives of hyperthermophiles, PNAS 97, 14421-14426, 2000.

Schouten, S., Hopmans, E. C., Schefuß, E., and Sinninghe Damsté, J. S.: Distributional variations in marine crenarchaeotal membrane lipids: A new tool for reconstructing ancient sea water temperatures?, Earth. Planet. Sci. Lett., 204, 265-274, 2002.

Schouten, S., Hopmans, E. C., and Sinninghe Damsté, J. S.: The effect of maturity and depositional redox conditions on archaeal tetraether lipid palaeothermometry, Org. Geochem., 35, 567-571, 2004.

Schouten, S., Huguet, C., Hopmans, E. C., Kienhuis, M. V. M., and Sinninghe Damsté, J. S.: Analytical methodology for $TEX_{86}$ paleothermometry by high-performance liquid chromatography/atmospheric pressure chemical ionization-mass spectrometry, Anal. Chem., 79, 2940-2944, 2007.

Schouten, S., Pitcher, A., Hopmans, E. C., Villanueva, L., van Bleijswijk J., and Sinninghe Damsté, J. S.: Intact polar and core glycerol dibiphytanyl glycerol tetraether lipids in the Arabian Sea oxygen minimum zone: I. Selective preservation and degradation in the water column and consequences for the $TEX_{86}$, Geochim. Cosmochim. Acta, 98, 228-243, 2012.

Schouten, S., Hopmans, E. C., and Sinninghe Damsté, J. S.: The organic geochemistry of glycerol dialkyl glycerol tetraether lipids: A review, Org. Geochem., 54, 19-61, 2013.

Seki, O., Nakatsuka, T., Kawamura, K., Saitoh, S.-I., and Wakatsuchi, M.: Time-series sediment trap record of alkenones from the western Sea of Okhotsk. Mar. Chem., 104, 253-265, 2007.

Sell, D. W., and Evans, M. S.: A statistical analysis of subsampling and an evaluation of the Folsom plankton splitter, Hydrobiologia, 94, 223-230, 1982.

Shah, S. R., Mollenhauer, G., Ohkouchi, N., Eglinton, T. I., and Pearson, A.: Origins of archaeal tetraether lipids in sediments: insights from radiocarbon analysis, Geochim. Cosmochim. Acta, 72, 4577-4594, 2008.

Sicre, M. -A., Bard, E., Ezat, U., and Rostek, F.: Alkenone distributions in the North Atlantic and Nordic sea surface waters, Geochem., Geophys., Geosyst., 3, 1-13, 2002.

Sicre, M. -A., Labeyrie, L., Ezat, U., Duprat, J., Turon, J. -L., Schmidt, S., Michel, E., and Mazaud, A.: Mid-Latitude southern ocean response to northern hemisphere Heinrich events, Earth Planet. Sci. Lett., 240, 724-731, 2005.

Sicre, M. -A., Labeyrie, L., Ezat, U., Duprat, J., Turon, J. -L., Schmidt, S., Michel, E., and Mazaud, A.: Erratum to: Mid-Latitude southern ocean response to northern hemisphere Heinrich events, Earth Planet. Sci. Lett., 243, 303-304, 2006.

Sigtryggsson, H.: An outline of sea ice conditions in the vicinity of Iceland, Jökull, 22, 1-11, 1972.

Sikes, E. L., and Volkman, J. K.: Calibration of alkenone unsaturation ratios ($U^{K'}_{37}$) for paleotemperature estimation in cold polar waters, Geochim. Cosmochim. Acta, 57, 1883-1889, 1993.

838 Sikes, E. L., Volkman, J. K., Robertson, L. G., and Pichon, J. -J.: Alkenones and alkenes in surface
839 waters and sediments of the Southern Ocean: implications for paleotemperature estimation in
840 polar regions, Geochim. Cosmochim. Acta, 61, 1495-1505, 1997.
841 Sikes, E. L., O'Leary, T., Nodder, S. D., and Volkman, J. K.: Alkenone temperature records and
842 biomarker flux at the subtropical front on the Chatham rise, SW Pacific Ocean. Deep-Sea Res.
843 Pt I, 52, 721-748, 2005.
844 Sinninghe Damsté, J. S., Hopmans, E. C., Schouten, S., van Duin, A. C. T., and Geenevasen, J. A.
845 J.: Crenarchaeol: the characteristic core glycerol dibiphytanyl glycerol tetraether membrane
846 lipid of cosmopolitan pelagic crenarchaeota, J. Lipid Res., 43, 1641-1651, 2002.
847 Sinninghe Damsté, J. S., Rampen, S. W., Rijpstra, W. I. C., Abbas, B., Muyzer, G., and Schouten,
848 S.: A diatomaceous origin for long-chain diols and mid-chain hydroxy methyl alkanoates
849 widely occurring in Quaternary marine sediments: Indicators for high nutrient conditions,
850 Geochim. Cosmochim. Acta, 67, 1339-1348, 2003.
851 Smith, M., De Deckker, P., Rogers, J., Brocks, J., Hope, J., Schmidt, S., Lopes dos Santos, R., and
852 Schouten, S.: Comparison of $U^{K'}_{37}$, $TEX^{H}_{86}$ and LDI temperature proxies for reconstruction of
853 south-east Australian ocean temperatures, Org. Geochem., 64, 94-104, 2013.
854 Ternois, Y., Sicre, M.-A., Boireau, A., Conte, M. H., and Eglinton, G.: Evaluation of long-chain
855 alkenones as paleo-temperature indicators in the Mediterranean Sea. Deep-Sea Res. Pt I, 44,
856 271-286, 1997.
857 Ternois, Y., Sicre, M. -A., Boireau, A., Beaufort, L., Miquel, J. -C., and Jeandel, C.: Hydrocarbons,
858 sterols and alkenones in sinking particles in the Indian sector of the Southern Ocean, Org.
859 Geochem., 28, 489-501, 1998.
860 Thordardottir, Th.: Timing and duration of spring blooming south and southwest of Iceland, in: The
861 Role of Freshwater Outflow in Coastal Marine Ecosystems, NATO ASI Series, vol. G7,
862 Skreslet, S. (Ed.), Springer, Berlin, pp. 345-360, 1986.
863 Versteegh, G. J. M., Bosch, H. J., and de Leeuw, J. W.: Potential palaeoenvironmental information
864 of $C_{24}$ to $C_{36}$ mid-chain diols, keto-ols and mid-chain hydroxy fatty acids; a critical review,
865 Org. Geochem., 27, 1-13, 1997.
866 Versteegh, G. J. M., Jansen, J. H. F., de Leeuw, J. W., and Schneider, R. R.: Mid-chain diols and
867 keto-ols in SE Atlantic sediments: a new tool for tracing past sea surface water masses?,
868 Geochim. Cosmochim. Acta, 64, 1879-1892, 2000.
869 Volkman, J. K., Eglinton, G., Corner, E. D. S., and Forsberg, T. E. V.: Long-chain alkenes and
870 alkenones in the marine coccolithophorid *Emiliania huxleyi*. Phytochemistry, 19, 2619-2622,
871 1980.
872 Volkman, J. K., Barrett, S. M., Dunstan, G. A., and Jeffrey, S. W.: $C_{30}$-$C_{32}$ alkyl diols and
873 unsaturated alcohols in microalgae of the class Eustigmatophyceae, Org. Geochem., 18, 131-
874 138, 1992.

Volkman, J. K., Barrett, S. M., Blackburn, S. I., and Sikes, E. L.: Alkenones in *Gephyrocapsa oceanica*: implications for studies of paleoclimate, Geochim. Cosmochim. Acta, 59, 513-520, 1995.

Volkman, J. K., Barrett, S. M., and Blackburn, S. I.: Eustigmatophyte microalgae are potential sources of $C_{29}$ sterols, $C_{22}$ - $C_{28}$ n-alcohols and $C_{28}$ - $C_{32}$ n-alkyl diols in freshwater environments, Org. Geochem., 30, 307-318, 1999.

Weijers, J. W. H., Schouten, S., Spaargaren, O. C., and Sinninghe Damsté, J. S.: Occurrence and distribution of tetraether membrane lipids in soils: implications for the use of the $TEX_{86}$ proxy and the BIT index, Org. Geochem., 37, 1680-1693, 2006.

Weijers, J. W. H., Schouten, S., Schefuß, E., Schneider, R. R., and Sinninghe Damsté, J. S.: Disentangling marine, soil and plant organic carbon contributions to continental margin sediments: a multiproxy approach in a 20,000 year sediment record from the Congo deep-sea fan, Geochim. Cosmochim. Acta, 73, 119-132, 2009.

Wuchter, C., Abbas, B., Coolen, M. J. L., Herfort, L., van Bleijswijk, J., Timmers, P., Strous, M., Teira, E., Herndl, G. J., Middelburg, J. J., Schouten, S., and Sinninghe Damsté, J. S.: Archaeal nitrification in the ocean, PNAS, 103, 12317-12322, 2006.

Yamamoto, M., Shimamoto, A., Fukuhara, T., Naraoka, H., Tanaka, Y., and Nishimura, A.: Seasonal and depth variations in molecular and isotopic alkenone composition of sinking particles from the western North Pacific. Deep-Sea Res. Pt I, 54, 1571-1592, 2007.

Zhai, L., Gudmundsson, K., Miller, P., Peng, W., Gujfinnsson, H., Debes, H., Hátún, H., White III, G. N., Hernández Walls, R., Sathyendranath, S., and Platt, T.: Phytoplankton phenology and production around Iceland and Faroes. Cont. Shelf Res. 37, 15-25, 2012.

**Table 1.** Location, depth and other information of each material collected at different stations around Iceland.

| Station | Latitude | Longitude | Depth (m.b.s.l.) | Core length (cm) | Volume pumped (l) |
|---|---|---|---|---|---|
| *Sediment trap* | | | | | |
| 1 | N 61° 59.757' | W 16° 00.191' | Trap top failed<br>Trap bottom 1850 | | |
| *SPM collected around Iceland July 2011* | | | | | |
| 1 | N 62° 0.008' | W 16° 0.016' | 5 | | no data |
| 7 | N 61° 29.917' | W 24° 10.333' | 5 | | 26 |
| 8 | N 64° 17.583' | W 24° 8.811' | 5 | | 25 |
| 10 | N 66° 40.647' | W 24° 10.794' | 5 | | 130 |
| 13 | N 67° 30.098' | W 15° 4.109' | 5 | | 164 |
| 16 | N 63° 59.132' | W 12° 12.472' | 6 | | 10 |
| SPM collected along transect July 2012 | | | | | |
| A | N 61° 59.757' | W 16° 00.191' | 20 | | 36 |
| A | N 61° 59.757' | W 16° 00.191' | 50 | | 229 |
| B | N 62° 14.963' | W 16° 51.877' | 50 | | 199 |
| C | N 62° 29.635' | W 17° 50.287' | 50 | | 183 |
| D | N 62° 44.568' | W 18° 48.771' | 50 | | 216 |
| E | N 62° 58.981' | W 19° 47.270' | 50 | | 220 |
| F | N 63° 12.696' | W 20° 44.820' | 50 | | 219 |
| G | N 63° 27.319' | W 21° 44.951' | 50 | | 219 |
| *Sediment cores* | | | | | |
| 1 | N 62° 0.019' | W 15° 59.951' | 2255 | 18 | |
| 3 | N 63° 21.972' | W 16° 37.696' | 240 | 5 | |
| 5 | N 63° 34.996' | W 22° 8.624' | 188 | 15 | |
| 6 | N 63° 14.294' | W 22° 33.685' | 315 | 15 | |
| 7 | N 61° 29.913' | W 24° 10.335' | 1628 | 28 | |
| 8 | N 64° 17.591' | W 24° 8.825' | 260 | 33 | |
| 10 | N 66° 40.647' | W 24° 10.770' | 241 | 30 | |
| 11 | N 66° 37.999' | W 20° 50.006' | 367 | 10 | |
| 13 | N 67° 30.098' | W 15° 4.153' | 884 | 10 | |
| 14 | N 66° 18.186' | W 13° 58.369' | 262 | no data | |

**Table 2.** Sampling intervals in the sediment trap, and fluxes of lipids. For proxy values and derived temperatures see Supplementary Table S1.

| Start sampling (mm/dd/yy) | Sampling interval (days) | Bulk flux flux (mg $m^{-2}$ $day^{-1}$) | $C_{37:2}$+$C_{37:3}$ flux (µg $m^{-2}$ $day^{-1}$) | GDGT-0 flux (µg $m^{-2}$ $day^{-1}$) | GDGTs-$TEX_{86}$ flux (µg $m^{-2}$ $day^{-1}$) | Crenarchaeol flux (µg $m^{-2}$ $day^{-1}$) | 1,14-diols flux (ng $m^{-2}$ $day^{-1}$) | unsat. 1,14-diols flux (ng $m^{-2}$ $day^{-1}$) | LDI-diol flux (ng $m^{-2}$ $day^{-1}$) |
|---|---|---|---|---|---|---|---|---|---|
| 1 (07/15/11) | 16.5 | 166 | 115 | 2756 | 645 | 2617 | 498 | 282 | 160 |
| 2 (08/01/11) | 17.5 | 9.3 | 0.91 | 220 | 52.5 | 174 | 32 | 0 | 10.7 |
| 3 (08/19/11) | 17.5 | 21 | 0.32 | 275 | 54.5 | 240 | 13.6 | 2.8 | 4.8 |
| 4 (09/05/11) | 17.5 | 75 | 1.03 | 3043 | 546 | 2863 | 546 | 3719 | 120 |
| 5 (09/23/11) | 17.5 | 118 | – | 2582 | 609 | 2607 | 767 | 1624 | 147 |
| 6 (10/10/11) | 17.5 | 49 | 1.04 | 1960 | 384 | 1767 | 452 | 534 | 96 |
| 7 (10/27/11) | 17.5 | 7.5 | 0.10 | 367 | 94 | 332 | 23 | 2 | 6.3 |
| 8 (11/14/11) | 17.5 | 28 | 0.11 | 435 | 132 | 388 | 33.2 | 52 | 7.4 |
| 9 (12/01/11) | 17.5 | 28 | 0.32 | 1169 | 384 | 1127 | 86 | 154 | 28.5 |
| 10 (12/19/11) | 17.5 | 16.8 | 0.27 | 602 | 222 | 592 | 31.2 | 49 | 11 |
| 11 (01/05/12) | 17.5 | 16.6 | 0.18 | 722 | 274 | 715 | 57 | 85 | 16.2 |
| 12 (01/23/12) | 17.5 | 11.2 | 0.20 | 759 | 297 | 737 | 46 | 0 | 12 |
| 13 (02/09/12) | 17.5 | 11.2 | 0.21 | 902 | 343.4 | 885 | 40.5 | 59 | 19.2 |
| 14 (02/26/12) | 17.5 | 9.3 | 0.12 | 414 | 159 | 392 | 33 | 45 | 9 |
| 15 (03/15/12) | 17.5 | 18.6 | 0.02 | 279 | 83 | 198 | 41.4 | 20 | 35 |
| 16 (04/01/12) | 17.5 | 7.5 | 0.08 | 392 | 156 | 374 | 6.8 | 3.4 | 2.3 |
| 17 (04/19/12) | 17.5 | 3.7 | 0.04 | 173 | 64 | 163 | 3.8 | 5.1 | 1.5 |
| 18 (05/06/12) | 17.5 | 108 | 53.5 | 4870 | 687 | 3965 | 536 | 421 | 165 |
| 19 (05/24/12) | 17.5 | 160 | 134 | 14446 | 2335 | 10979 | 407 | 467 | 155 |
| 20 (06/10/12) | 17.5 | 134 | 74 | 10895 | 1971 | 9710 | 185 | 256 | 106 |
| 21 (06/27/12) | 17.5 | 45 | 2.6 | 1867 | 381.1 | 1548 | 33 | 32 | 9.8 |

**Table 3.** Proxy derived temperatures at Station 1 at the northern part of Iceland basin in sedimenting particles and surface sediment and measured temperature data from satellite observations (AVHRR, NOAA) and from the climate database WOA09 (Locarnini et al., 2010).

| | $U^{K'}_{37}$ | $TEX_{86}$ | $TEX^{L}_{86}$ | $TEX^{L}_{86}$ 0-200 m | LDI | Measured |
|---|---|---|---|---|---|---|
| Flux-weighted mean | 7.1 | 8.5 | 14.5 | 11.7 | -2.7 | |
| Surface sediment | 10.7 | 9.2 | 14 | 11.4 | -1.3 | |
| SPM July 2011, 5 m | 10.8 | 13.4 | 11.1 | – | – | |
| SMP July 2012, 20 m | 12.4 | 14.4 | 8.8 | – | 3.4 | |
| Satellite July 2011, 5 m | | | | | | 11.3 |
| Satellite July 2012 20 m | | | | | | 12.9 |
| WOA09 annual mean 0m | | | | | | 9.4 |
| WOA09 annual mean 0-200 m | | | | | | 8.7 |

**Figure captions**

**Figure 1.** Bathymetric map of the study area with the location of the different sampling stations around Iceland. Filled circles indicates surface sediment stations with different color according to the area of location, i.e. yellow and green circles for the northern stations, red circles for the shallow stations in the south of Iceland and blue circles for the deep southern stations. Black and blue inverse triangles with filled circles indicate surface particulate matter stations around Iceland sampled during July 2011 and transect from Iceland Basin (St A) to Reykjavik (St G) samples. during July 2012, respectively. The red star indicates the location of sediment trap deployment. Dashed blue lines show the theoretical circulation of the different water masses.

**Figure 2.** $U^{K'}_{37}$-, $TEX^{L}_{86}$- and LDI-derived temperatures from SPM obtained at the different sampling stations around Iceland . (a) SPM collected at ca. 5 m water depth during July 2011; (b) SPM collected at 50 m water depth collected during July 2012. Open green diamonds indicate $U^{K'}_{37}$-derived temperatures; filled dark blue circles indicate $TEX_{86}$-derived temperatures using calibration by Kim et al. (2010a); open blue circles indicate $TEX^{L}_{86}$-derived temperatures using calibration by Kim et al. (2010a); open brown squares indicate LDI-derived temperatures. Orange symbols indicate in situ SST measured with the CTD, pink symbols indicate satellite SST from NOAA remote sensing records at the time period of collection of the samples, i.e. July 2011 and July 2012, and purple symbols indicate summer mean temperatures at 50 m water depth from WOA09 database.

**Figure 3.** (a) Variations in the net primary productivity from July 2011 to July 2012 derived from Ocean Color Web (Behrenfeld and Falkowski, 1997a). Bar plots of fluxes of (b) bulk sediment, (c) $C_{37}$ alkenones, (d) isoprenoid GDGTs, and (e) long chain diols as determined from sediment trap data. Numbers refer to sampling intervals specified in Table 2.

**Figure 4.** Changes in $U^{K'}_{37}$- (green line and diamonds), $TEX_{86}$- (dark blue line and open circles), $TEX^{L}_{86}$- (light blue line and open circles), $TEX^{L}_{86}$- 0-200 m (light red line and open circles), and LDI- (brown line and open squares) derived temperatures in descending particles over one complete annual cycle, from July 2011 to July 2012. Numbers refer to sampling intervals specified in Table 2, and data points represent the center of collection intervals. Satellite temperatures (from AVHRR, NOAA) at St 1 during the sampling period

1014 are indicated with a dashed orange line and 0-200 mean temperatures from WOA09 are
1015 indicated with a dashed purple line.
1016
1017 **Figure 5.** $U^{K'}_{37}$- (open green diamonds), $TEX_{86}$- (dark blue circles), $TEX^{L}_{86}$- (open light
1018 blue circles), $TEX^{L}_{86}$ 0-200 m (open red circles) and LDI- (open brown squares) derived
1019 temperatures in surface sediments from stations around Iceland. Annual mean SSTs at each
1020 station obtained from the WOA09 database are indicated as purple crosses.
1021
1022 **Figure 6.** Cross-plots of surface sediment proxy-derived temperatures ($U^{K'}_{37}$-, $TEX_{86}$-,
1023 $TEX^{L}_{86}$-, $TEX^{L}_{86}$ 0-200 m and LDI-) with annual and seasonal mean temperatures (only the
1024 best seasonal correlations are shown) from the WOA09 database. Regression lines are
1025 represented as black lines, and diagonal black dashed lines show the 1:1 correlation.
1026 Different color codes indicate different station locations according to Figure 1.

**Fig. 1**

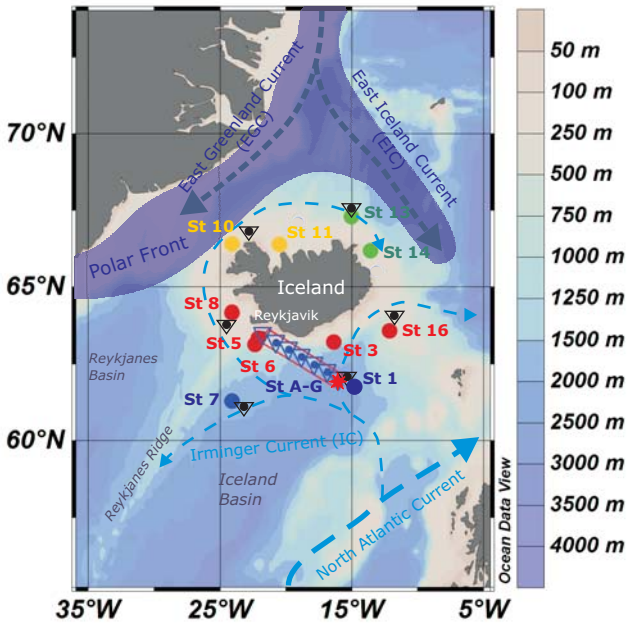
70°N
65°N
60°N
35°W
25°W
15°W
5°W
East Greenland Current (EGC)
East Iceland Current (EIC)
Polar Front
Iceland
Reykjavik
St 10
St 11
St 12
St 14
St 8
St 5
St 6
St A-G
St 3
St 16
St 1
St 7
Reykjanes Basin
Iceland Basin
Reykjanes Ridge
Irminger Current (IC)
North Atlantic Current
Ocean Data View
50 m
100 m
250 m
500 m
750 m
1000 m
1250 m
1500 m
2000 m
2500 m
3000 m
3500 m
4000 m

**Fig. 2**

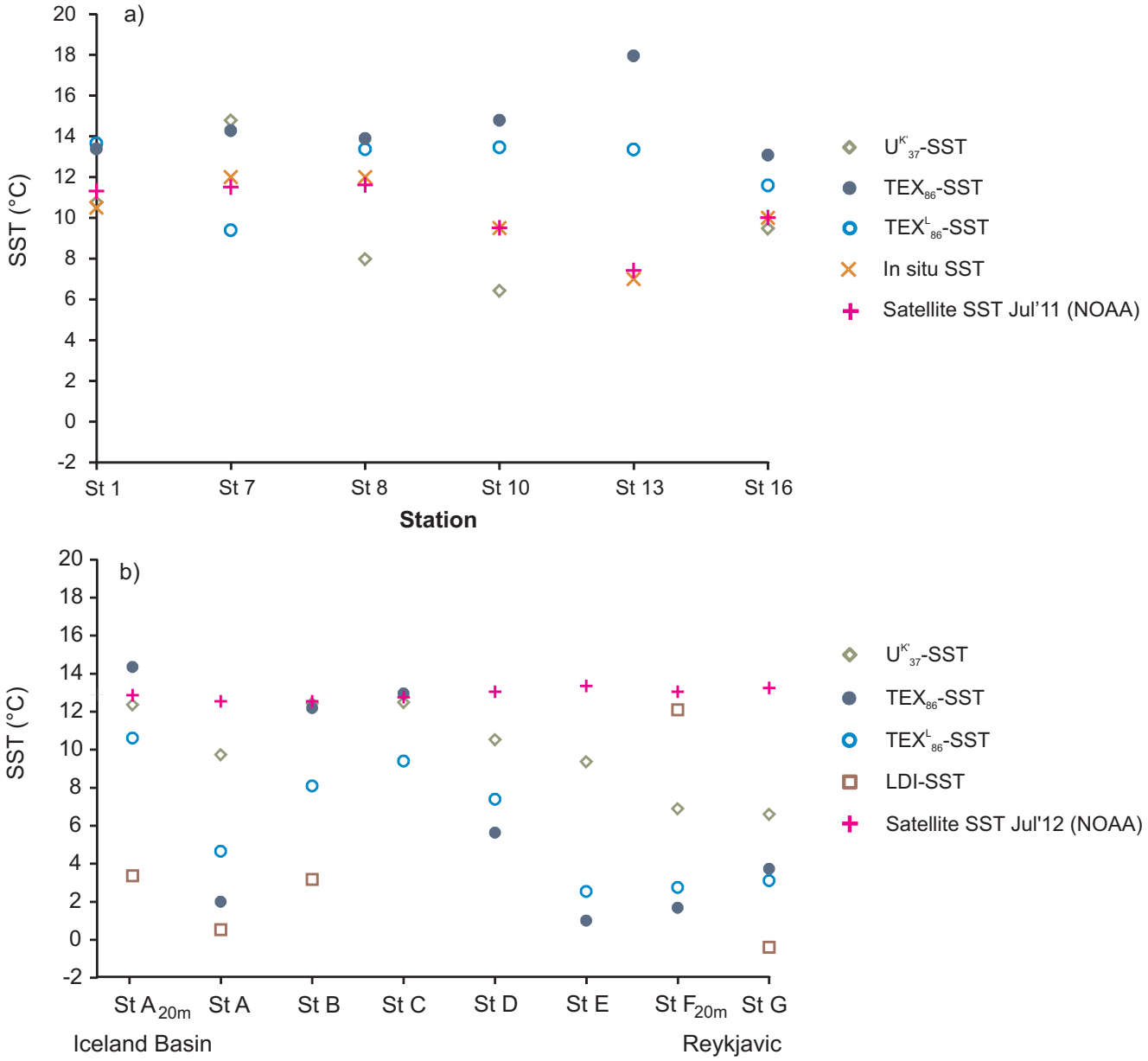
a)
SST (°C)
20
18
16
14
12
10
8
6
4
2
0
-2
St 1
St 7
St 8
St 10
St 13
St 16
Station
$U^{K'}_{37}$-SST
$TEX_{86}$-SST
$TEX^{L}_{86}$-SST
In situ SST
Satellite SST Jul'11 (NOAA)
b)
SST (°C)
St $A_{20m}$
St A
St B
St C
St D
St E
St $F_{20m}$
St G
Iceland Basin
Reykjavic
$U^{K'}_{37}$-SST
$TEX_{86}$-SST
$TEX^{L}_{86}$-SST
LDI-SST
Satellite SST Jul'12 (NOAA)

**Fig. 3**

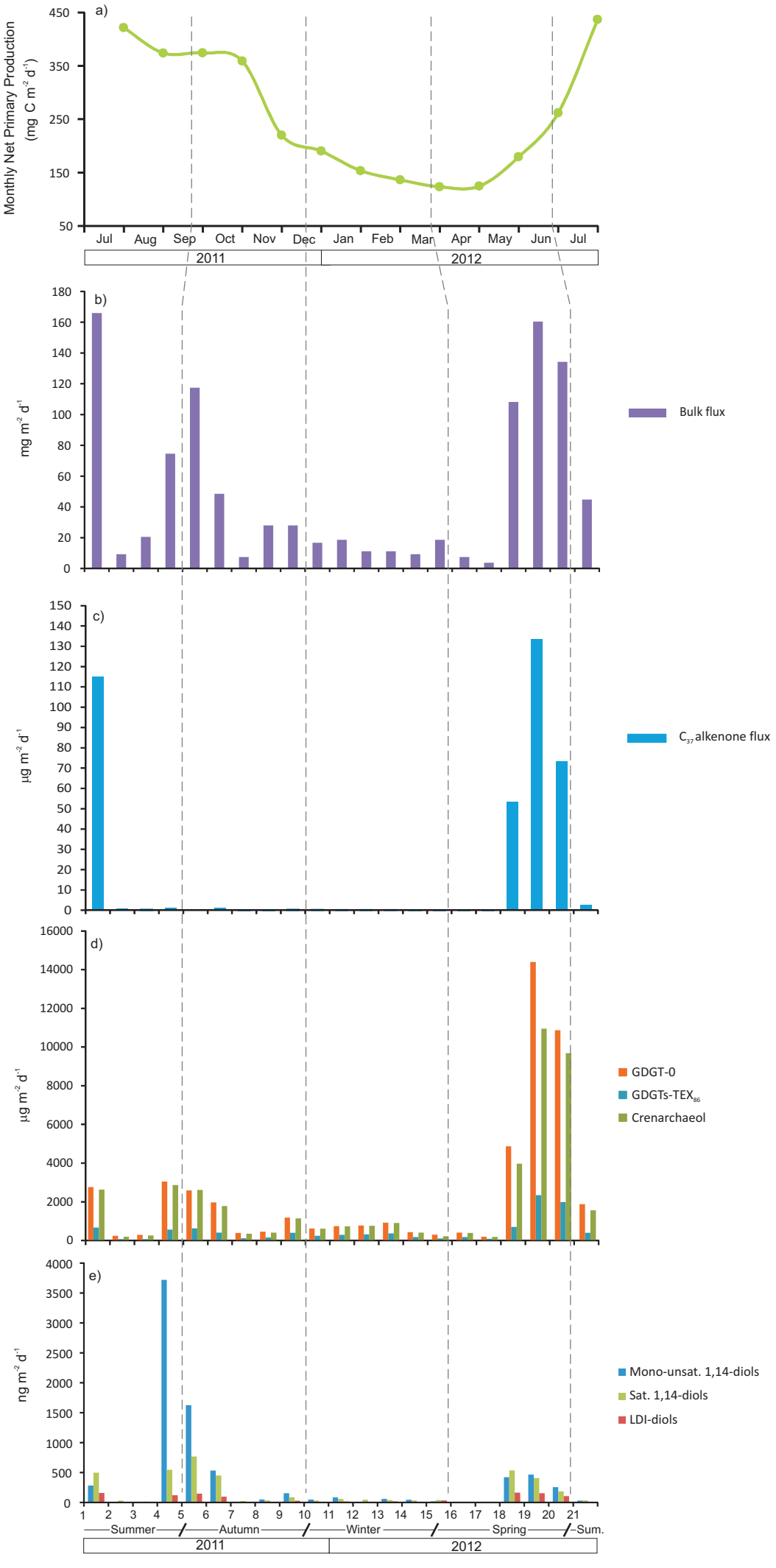
a)
Monthly Net Primary Production (mg C m-2 d-1)
450
350
250
150
50
Jul
Aug
Sep
Oct
Nov
Dec
Jan
Feb
Mar
Apr
May
Jun
Jul
2011
2012
b)
mg m-2 d-1
180
160
140
120
100
80
60
40
20
0
Bulk flux
c)
µg m-2 d-1
150
140
130
120
110
100
90
80
70
60
50
40
30
20
10
0
C37 alkenone flux
d)
µg m-2 d-1
16000
14000
12000
10000
8000
6000
4000
2000
0
GDGT-0
GDGTs-TEX86
Crenarchaeol
e)
ng m-2 d-1
4000
3500
3000
2500
2000
1500
1000
500
0
Mono-unsat. 1,14-diols
Sat. 1,14-diols
LDI-diols
1
2
3
4
5
6
7
8
9
10
11
12
13
14
15
16
17
18
19
20
21
Summer
Autumn
Winter
Spring
Sum.
2011
2012

**Fig. 4**

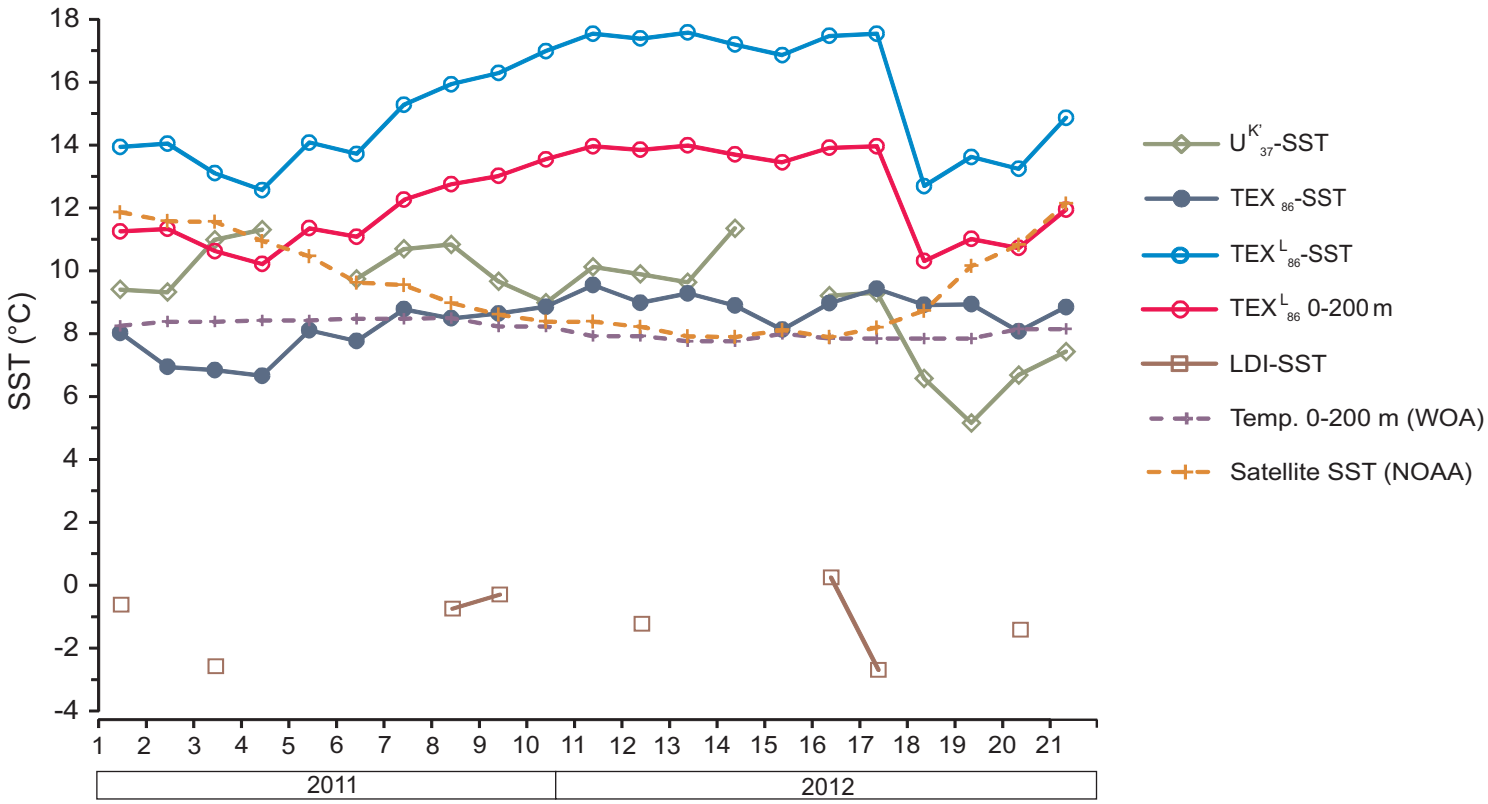
SST (°C)
18
16
14
12
10
8
6
4
2
0
-2
-4
1 2 3 4 5 6 7 8 9 10 11 12 13 14 15 16 17 18 19 20 21
2011
2012
U^K'37-SST
TEX86-SST
TEX^L86-SST
TEX^L86 0-200 m
LDI-SST
Temp. 0-200 m (WOA)
Satellite SST (NOAA)

**Fig. 5**

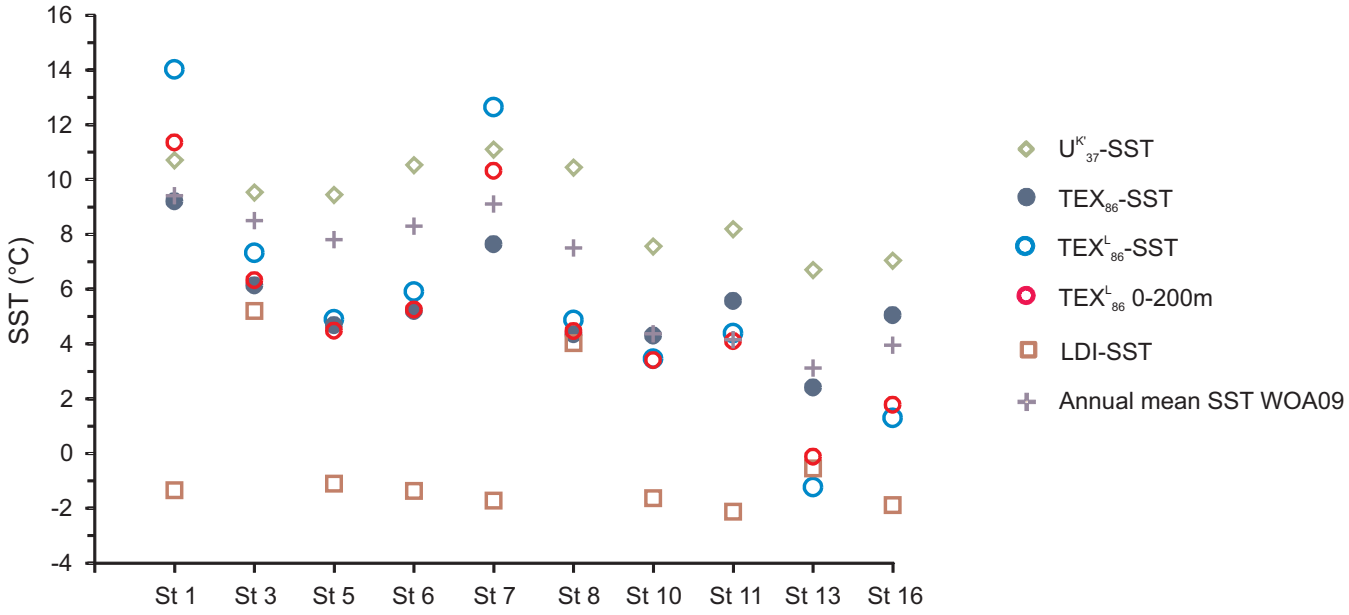
SST (°C)
16
14
12
10
8
6
4
2
0
-2
-4
St 1
St 3
St 5
St 6
St 7
St 8
St 10
St 11
St 13
St 16
$U^{K'}_{37}$-SST
$TEX_{86}$-SST
$TEX^{L}_{86}$-SST
$TEX^{L}_{86}$ 0-200m
LDI-SST
Annual mean SST WOA09

Fig. 6

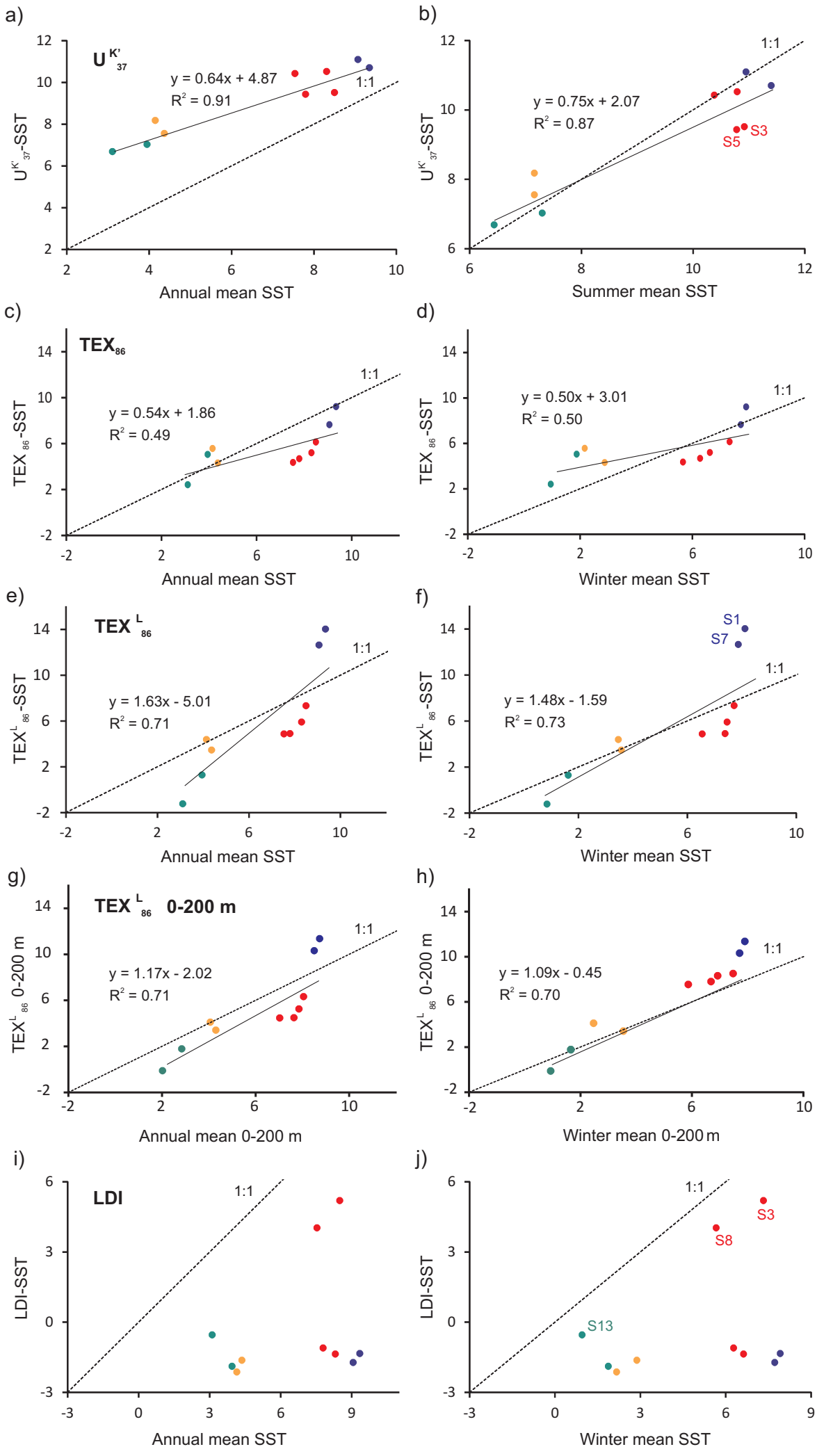
a)
$U^{K'}_{37}$
y = 0.64x + 4.87
$R^2$ = 0.91
1:1
$U^{K'}_{37}$-SST
Annual mean SST
b)
1:1
y = 0.75x + 2.07
$R^2$ = 0.87
S5
S3
$U^{K'}_{37}$-SST
Summer mean SST
c)
$TEX_{86}$
1:1
y = 0.54x + 1.86
$R^2$ = 0.49
$TEX_{86}$-SST
Annual mean SST
d)
1:1
y = 0.50x + 3.01
$R^2$ = 0.50
$TEX_{86}$-SST
Winter mean SST
e)
$TEX^L_{86}$
1:1
y = 1.63x - 5.01
$R^2$ = 0.71
$TEX^L_{86}$-SST
Annual mean SST
f)
S1
S7
1:1
y = 1.48x - 1.59
$R^2$ = 0.73
$TEX^L_{86}$-SST
Winter mean SST
g)
$TEX^L_{86}$ 0-200 m
1:1
y = 1.17x - 2.02
$R^2$ = 0.71
$TEX^L_{86}$ 0-200 m
Annual mean 0-200 m
h)
1:1
y = 1.09x - 0.45
$R^2$ = 0.70
$TEX^L_{86}$ 0-200 m
Winter mean 0-200 m
i)
LDI
1:1
LDI-SST
Annual mean SST
j)
1:1
S3
S8
S13
LDI-SST
Winter mean SST